Cerebral Cortex, 2017; 1–19

doi: 10.1093/cercor/bhx145
Original Article

ORIGINAL ARTICLE

Histamine Enhances Theta-Coupled Spiking and Gamma Oscillations in the Medial Entorhinal Cortex Consistent With Successful Spatial Recognition

Quanhui Chen[1], Fenlan Luo[1], Faguo Yue[1], Jianxia Xia[1], Qin Xiao[1], Xiang Liao[2], Jun Jiang[3], Jun Zhang[1], Bo Hu[1], Dong Gao[4], Chao He[1] and Zhian Hu[1]

[1]Department of Physiology, Collaborative Innovation Center for Brain Science, Third Military Medical University, Chongqing 400038, China, [2]Brain Research Center, Third Military Medical University, Chongqing 400038, China, [3]Department of Basic Psychology, School of Psychology, Third Military Medical University, Chongqing 400038, China and [4]Department of Sleep and Psychology, Institute of Surgery Research, Daping Hospital, Third Military Medical University, Chongqing 400042, China

Address correspondence to Zhian Hu, Department of Physiology, Collaborative Innovation Center for Brain Science, Third Military Medical University, No. 30, Gaotanyan Street, Shapingba District, Chongqing 400038, China. Email: zhianhu@aliyun.com; Chao He, Department of Physiology, Collaborative Innovation Center for Brain Science, Third Military Medical University, No. 30, Gaotanyan Street, Shapingba District, Chongqing 400038, China. Email: hechaochongqing@163.com and Dong Gao, Department of Sleep and Psychology, Institute of Surgery Research, Daping Hospital, Changjiang Road No. 10, Yuzhong District, Chongqing 400042, China. Email: gaodong1973@163.com

Abstract

Encoding of spatial information in the superficial layers of the medial entorhinal cortex (sMEC) involves theta-modulated spiking and gamma oscillations, as well as spatially tuned grid cells and border cells. Little is known about the role of the arousal-promoting histaminergic system in the modification of information encoded in the sMEC in vivo, and how such histamine-regulated information correlates with behavioral functions. Here, we show that histamine upregulates the neural excitability of a significant proportion of neurons (16.32%, 39.18%, and 52.94% at 30 μM, 300 μM, and 3 mM, respectively) and increases local theta (4–12 Hz) and gamma power (low: 25–48 Hz; high: 60–120 Hz) in the sMEC, through activation of histamine receptor types 1 and 3. During spatial exploration, the strength of theta-modulated firing of putative principal neurons and high gamma oscillations is enhanced about 2-fold by histamine. The histamine-mediated increase of theta phase-locking of spikes and high gamma power is consistent with successful spatial recognition. These results, for the first time, reveal possible mechanisms involving the arousal-promoting histaminergic system in the modulation of spatial cognition.

Key words: entorhinal cortex, histamine, spatial exploration, theta phase-locking, theta–gamma coupling

Introduction

Recent decades have witnessed breakthroughs in the characterization of spatial information encoding in the superficial layers of the medial entorhinal cortex (sMEC). During spatial exploration, the firing of putative principal neurons in the sMEC is tightly locked to local theta oscillations (Chrobak and Buzsaki 1994), and belongs to the underlying mechanism for temporal coordination between the entorhinal cortex and the

hippocampus (Mizuseki et al. 2009). Additionally, local gamma (40–100 Hz) oscillatory power is modulated by the theta (4–12 Hz) phase (Chrobak and Buzsaki 1998; Quilichini et al. 2010). Recently, neurons carrying spatial cues have been found in the sMEC, especially the typical grid cells (Fyhn et al. 2004; Hafting et al. 2005) and border cells (Solstad et al. 2008). The activity of grid cells, but not border cells, is tightly regulated by theta phase-locking and theta–nested gamma oscillations (Pastoll et al. 2013; Ray et al. 2014; Tang et al. 2014).

It is well known that neural excitability and synaptic transmission are modified by arousal-promoting systems, such as the cholinergic, histaminergic, noradrenergic, and dopaminergic systems (Xiao et al. 2009a, 2009b; Cilz et al. 2014; He et al. 2016). Histaminergic neurons are exclusively located in the tuberomammillary nucleus of the hypothalamus (Thakkar 2011; Panula and Nuutinen 2013; Zha and Xu 2015), and project fibers throughout the brain, playing an important role in maintaining wakefulness (Lin et al. 2011). The activity of histaminergic neurons is high during wakefulness, but extremely low during sleep (Lin 2000). Disruption of histaminergic neurons or their receptors impairs arousal (Thakkar 2011; Panula and Nuutinen 2013). The importance of arousal-promoting systems in cognition has been extensively studied in respect to the hippocampus and medial prefrontal cortex (Otani et al. 2015; Wang et al. 2015; Ballinger et al. 2016). By contrast, how the encoding of spatial information in the sMEC and corresponding behavioral functions are modulated by arousal systems is poorly understood. The arousal-promoting systems project dense fibers to the sMEC, and their receptors have also been detected. In vitro studies demonstrated a role for these neurotransmitters in the regulation of neural activities in the sMEC (Xiao et al. 2009b; Cilz et al. 2014; He et al. 2016). These earlier evidences strongly suggested that the ongoing encoding of information in the sMEC is probably modulated by arousal-promoting systems. Indeed, the encoding of grid cells relies on cholinergic input. Systemic blocking of muscarinic receptors disrupts the spatial tuning of grid cells (Newman et al. 2014), and specifically reduces the strength of theta modulation of trough-locked grid cells (Newman and Hasselmo 2014). Moreover, cholinergic input enhances the coupling between theta phase and gamma amplitude, which in rats is correlated with high-speed modulation (Newman et al. 2013). At present, whether these individual arousal-promoting systems play different roles in information processing in the sMEC and its related functions remains unknown.

The histaminergic system is critical for spatial learning and memory (Haas et al. 2008; Panula and Nuutinen 2013), and histaminergic fibers have been detected in the sMEC (Airaksinen and Panula 1988; Panula et al. 1998). Our previous studies demonstrated superficially enriched expression of histamine receptors in the MEC, and histamine in vitro increases neuronal excitability and facilitates synaptic transmission, which is involved in accurate spatial learning (He et al. 2016). However, the role of the histaminergic system (especially in comparison with the cholinergic system) in regulating information encoded in the sMEC in vivo, and how this histamine-modulated information processing correlates with behavioral functions, needs to be further clarified.

In the present study, we used multichannel recordings and neuropharmacological techniques to explore the role of the histaminergic system in modulating the encoding of information in the sMEC, as well as modulation of sMEC-related behaviors. Compared with traditional single-unit electrophysiology, the multiple electrode array recording technique has several advantages in studies of neuroscience: (1) simultaneous recording of large-scale neural activities; (2) available mathematics to analyze massive neural data sets; and (3) it allows investigation of the relationship between neural activities and behaviors, and can reveal functional cells or oscillatory activities at behavioral levels (Buzsaki 2004). During spatial exploration, unlike with cholinergic input, histamine does not influence the encoding of grid cells and border cells. However, it enhances the theta phase-locking of putative principal neuronal firing and local high gamma oscillations via types 1 and 3 histamine receptors (H1Rs and H3Rs). Histamine-mediated theta modulation of spiking and high gamma power is correlated with successful spatial recognition. These results provide new insights into the regulatory role of the arousal-promoting histaminergic system during spatial learning and memory.

Materials and Methods

Subjects

A total of 37 male Sprague–Dawley rats (350–450 g at the time of surgery and behavioral tests) were used in this study. Two of these rats were implanted with a drug cannula at 30° in the sagittal plane (the tip of the cannula pointed to the posterior direction), and an electrode array perpendicular to the horizontal plane in the left sMEC. In 21 rats, a drug cannula and electrode were implanted in the left sMEC, as well as an additional vertical drug cannula in the right sMEC. In 14 rats, 2 drug cannulas were vertically implanted in the left and right sMEC. The rats were group-housed with food and water available ad libitum before surgery. The housing environment was kept on a 12 h light/dark cycle. All the experiments were conducted in the dark phase from 20:00 h to 24:00 h and were in strict accordance with the Third Military Medical University Guide for the Care and Use of Laboratory Animals. Only rats with stable recording during experiments, low baseline noises, and no 50 Hz power line interference were included in the analysis. During the recording of the free moving and spatial exploration test, the data from 3 rats were discarded because of unacceptable baseline noise.

Surgical Procedure

All surgical procedures were performed under aseptic conditions. Rats were anesthetized with 3% sodium pentobarbital (2.5 mL/kg, i.p.), with an additional dose (0.15 mL/h) being injected 2 h after the first administration.

For implantation of the drug cannula and electrode array in the left sMEC in 2 rats, the head of the rats was first fixed on a stereotactic frame (RWD Life Technology Co., Ltd). The incision site was cleaned using iodine and medical alcohol. The scalp and the periosteum were carefully removed to expose the skull surface. Then, with the help of a microscope, a bone window (1.5 × 1.5 mm) with a center at AP −8.3 mm and ML −4.6 mm (left side) and a small burr hole at AP −4.4 mm and ML −4.6 mm (left side) were made for implantation of electrode and guide cannula, respectively. In 21 rats, in addition to implantation of the drug cannula and electrode array in the left sMEC, another small burr hole at AP −8.3 mm and ML +4.6 mm (right side) was drilled for cannula implantation. After having carefully removed the dura in the small burr hole of both sides, the drug cannula was lowered to the sMEC (left: 5.2 mm, 30° in the sagittal plane with the tip of the cannula pointed to the posterior direction; right: 4.4 mm, vertical to the horizontal plane) at a speed of 5 μm/s, controlled by an automatic micromanipulator (IVM-1000, Scientifica, USA). Dental acrylic was used to preliminarily fix the cannulas. The electrode array was then slowly implanted into the sMEC from the center of the cranial window at a speed of

1 μm/s (depth: 4–4.5 mm). Once the electrode reached the targeted sMEC with a high signal-to-noise ratio of spike activities, a drop of agarose gel was carefully injected into the bone window to protect the brain tissue. Finally, the cannulas and electrodes were firmly fixed to the skull with dental acrylic.

The surgical steps for bilateral implantation of drug cannulas in the sMEC in 14 rats were similar to the aforementioned cannula implantation procedures. After carefully exposing the skull surface, 2 small holes were drilled with coordinates of AP −8.3 mm and ML ± 4.6 mm (left and right). The 2 drug cannulas were simultaneously lowered to the left and the right sMEC (depth: 4.4 mm) with the help of an automatic micromanipulator (IVM-1000, Scientifica). Dental acrylic was used to fully fix the cannulas to the skull.

Behavioral Recording

Freely Moving Test

After surgery, all rats were allowed 7–10 days for recovery, including 3–4 days of gentle acclimatization. Eleven freely behaving rats underwent in vivo recording of sMEC neural activities in a black open field (100 × 100 cm) polarized with a square white cue on one of the walls. After a baseline of 10 min of recording, drugs were slowly and unilaterally infused into the left sMEC. Another 30–40 min were recorded immediately after drug infusion to continuously investigate the effects of the drugs on neuronal activities in the sMEC. Ethanol (15%) was used to eliminate the influence of smell across different rats.

Spatial Exploration Test

After recovery from the surgery and before testing, rats underwent a food deprivation schedule until their body weight was approximately 85% of the initial free-feeding weight; this is a frequently used protocol in studies of spatial exploration (Sargolini et al. 2006; Solstad et al. 2008). This protocol took about 3–5 days, during which the rats received 3 g of food/day under food deprivation until they were approximately 85% of their initial weight. During the recording days, a fixed 10 g/day of food was given to maintain the 85% body weight. After 3 days of adaptation to the open field, the rats could freely explore the 2D environment with randomly scattered food. As for spatial exploration, we defined the periods only when rats actively explore the 2D environment with a running speed >5 cm/s for the data analyses (Tang et al. 2014, 2015). Data recorded during low-speed and immobility epochs were excluded from this study. First, rats underwent 15 min of running to record the baseline neural activities in the sMEC during spatial exploration in the open field. Then, drugs were slowly and bilaterally injected into the sMEC through the cannula. After 10 min of drug diffusion, rats were allowed to explore the open field for a second session of 15 min.

Spatial Recognition Task

Two spatial recognition tasks, which were used in previous studies (Van Cauter et al. 2013), were applied to investigate the role of the histaminergic system in spatial recognition. (1) One-trial recognition task: the 2D environment was the aforementioned open field. As illustrated in Figure 6*a*, rats were familiarized to the open field for 10 min on day 1. In the presentation phase on day 2, two objects were placed in the apparatus. Rats could freely explore the objects for 5 min. After a 5 min interval in the home cage, a 5 min test phase followed. In this test phase, the spatial position of one object was changed, and rats were allowed to re-explore the 2 objects. Similar to the spatial recognition test on day 2, rats underwent a novel object recognition task on day 3. All procedures were the same as in the spatial recognition task, except that one of the objects was replaced by a novel object in the test phase. (2) Object exploration task: in this task, rats were first acclimatized with one trial of adaptation to the open field. The subsequent 6 trials for exploration of 4 objects in the apparatus allowed the rats to recognize the initial spatial configuration of these 4 objects. In trial 8, the spatial position of one object was changed, and rats were allowed to explore the new spatial arrangement of these objects. The following trial replicated the former trial to allow the rats to reacclimatize to the new spatial configuration. In trial 10, one object in trial 9 was substituted by a novel object to test the performance of rats in novel object recognition. Every trial in this task lasted 5 min, with a 5 min interval between trials.

Data Acquisition and Analysis

The electrode array (Plexon) consisted of 8 insulated nichrome wires (30 μm in diameter, 100–250 kΩ). The distance between individual wires was 200 μm. Electrodes were connected to an 8-channel headstage with a preamplifier and an omniplex neural data acquisition system (Plexon). The neural activity was digitized at 40 kHz and band-pass filtered from 250 Hz to 6 kHz for spike analysis. The neural data recorded before and after drug infusion were merged by using PlexUtil version 4 (Plexon), to ensure that the analyzed effects on spikes were from the same single unit. Single-unit sorting was accomplished using standard sorting routines in the software Off-Line Sorter version 3 (Plexon), according to the methods used in previous studies (Lu et al. 2016; Yang et al. 2016). The template sorting method was used to finely distinguish every single unit under each channel. First, recorded signals less than 5 times the standard deviation (SD) were detected as spike events. According to the characteristics of detected waveforms, principal component (PC) analysis (Dejean et al. 2016) was performed by orthogonal transformation to extract the first 3 linearly uncorrelated PCs of these waveforms. The 3 PCs for every waveform were plotted in 3D coordinates. A supervised *k*-means clustering algorithm operating on the first 3 PCs was used to distinguish different single units. Waveforms with isolated clusters in the 3D space were considered as a single-unit recorded from the same neuron. This sorting result with a −5 SD detecting threshold was set as a template. Then, the spike events in the same channel were redetected with a threshold of −4 SD, and sorted with the −5 SD template. Neurons with a refractory period of spikes less than 2 ms were excluded (Harris et al. 2000). The local field potential (LFP) was digitized at 1 kHz and then low-pass filtered with a cutoff at 250 Hz. The motion of the rats in the open field was simultaneously recorded with a video camera (sampling rate, 30 Hz), and the trajectory was obtained by offline tracking of the rat in the video. All analyses of electrophysiology and video data were conducted offline using software custom-written in MATLAB 2014a (Mathworks).

Firing Rate and Power Spectral Density Analysis

In our experiments, 2 kinds of waveforms were detected as previously described: those emanating from the putative principal neurons with large spike width (trough to peak) and low firing frequency, and those from the interneurons with narrow waveforms and high firing rate (Frank et al. 2001; Fyhn et al. 2004; Solstad et al. 2008). Only the putative principal neurons were focused on in this study. The criteria to identify principal neurons were defined following previous study with spike width >0.4 ms and firing rate <16 Hz (Frank et al. 2001). For spike and LFP data, a

firing rate histogram and power spectral density (PSD) were first extracted using the software NeuroExplorer vision 4 (Plexon), before being analyzed using the MATLAB code. A drug response on firing rate was considered to be present when the change in the rate was larger than twice the SD of the baseline for at least 3 consecutive minutes, according to the rate–time curve (Haghparast et al. 2010). The PSD for each frequency band (delta: 0.5–4 Hz, theta: 4–12 Hz, beta: 12–25 Hz, low-frequency gamma [L-gamma]: 25–48 Hz, and high-frequency gamma [H-gamma]: 60–120 Hz) was normalized to the total power of the baseline trials. The division of gamma bands was based on previous studies (Colgin et al. 2009; Newman et al. 2013) and the results of theta–gamma coupling described below.

Grid Cell and Border Cell Analyses

The analyses of grid cells and border cells were performed according to previous studies (Fyhn et al. 2004; Solstad et al. 2008). Only spikes during running with a speed >5 cm/s and cells with a firing rate >0.5 Hz were included in the analyses (Tang et al. 2014, 2015). The 2D open field was divided into 2.5 × 2.5 cm bins (40 × 40 grid). The firing rate of individual neurons in each bin was calculated as follows:

$$\lambda(x) = \frac{\sum_{i=1}^{n} g\left(\frac{s_i - x}{h}\right)}{\int_0^T g\left(\frac{y(t) - x}{h}\right) dt}.$$

In the above equation, n is the number of spikes, s_i is the position of the ith spike, $y(t)$ is the location at time t, $[0, T]$ is the recording period, and g and h are the smoothing kernel and the smoothing factor, respectively. Here, a Gaussian kernel was used and $h = 5$ cm.

If a region was detected with an area >200 cm^2 and a firing rate >30% of the peak rate, it was defined as a firing field. The following parameters were used to evaluate the firing fields: (1) average rate, the mean firing rate during each trial; (2) peak rate, the maximal firing rate in the rate map; (3) mean field size, the average of all firing fields; and (4) the spatial information rate, indicating the contrast of the neuronal firing fields to the background. A neuron with a higher spatial information rate has higher spatially tuned firing fields. Sparsity implies the spacing of firing field distribution. A higher sparsity value means a more discrete spatial distribution of the firing fields. These 2 parameters were calculated according to the following formulas:

$$\text{Information rate} = \sum_i p_i \lambda_i \log_2 \frac{\lambda_i}{\lambda}$$

$$\text{Sparsity} = \frac{\lambda^2}{\sum_i p_i \lambda_i^2}$$

In the above formulas, p_i is the probability of rat running in the ith bin (time in the ith bin/recording duration); λ_i is the average rate in the ith bin; and λ is the mean firing rate during the whole trial.

According to the spatial firing maps, the autocorrelograms were calculated using Pearson's product moment correlation:

$$r(\tau_x, \tau_y) = \frac{n\sum\lambda(x, y)\lambda(x - \tau_x, y - \tau_y) - \sum\lambda(x, y)\sum\lambda(x - \tau_x, y - \tau_y)}{\sqrt{n\sum\lambda(x, y)^2 - (\sum\lambda(x, y))^2} \times \sqrt{n\sum\lambda(x - \tau_x, y - \tau_y)^2 - \left(\sum\lambda(x - \tau_x, y - \tau_y)\right)^2}},$$

where $\lambda(x, y)$, τ_x, and τ_y are the average rate and spatial lags at location (x, y), respectively.

To calculate the gridness score, the central peaks of the autocorrelogram were first sampled, and then the autocorrelogram was rotated for 60° and 120° (on peak), as well as 30°, 90°, and 150° (off peak). Pearson correlation was evaluated for the autocorrelogram and its rotations. The grid score was calculated as the minimum difference between the "on peak" and "off peak" rotations. A permutation test was performed to clarify the grid cells according to a previous study (Newman et al. 2014). The spiking times for each neuron were randomly assigned to the tracking position of the rat for 200 times, and thus generated a set of 200 permutated spike–trajectory maps. The grid scores for all of these 200 firing rate maps were calculated and a distribution of grid scores was obtained. Only neurons whose grid score for the original rate map exceeded the 95-percentile value of the permutated distribution of grid scores were considered as grid cells.

The borderness scores were defined by the following:

$$b = \frac{c_m - d_m}{c_m + d_m}.$$

In this formula, c_m is the maximum coverage of a firing field to 1 of the 4 walls of the open field, and d_m is the mean firing distance of a firing field. After normalizing the firing rate by the total pixels in the field, d_m was then normalized to half the length of the closest boundary. Similar permutation analysis was used to detect the threshold for border cells.

Theta Phase-Locking and Phase-Amplitude Coupling Analyses

Similar to the analyses in grid cells and border cells, spikes and LFP epochs for theta phase-locking and theta–gamma coupling analyses were included only when rats running with a speed >5 cm/s (Tang et al. 2014, 2015). The analyses of theta phase-locking and phase-amplitude coupling (PAC) were performed in accordance with widely used procedures (Tort et al. 2008, 2009; Tang et al. 2014, 2015). Briefly, the LFP was theta (4–12 Hz) band-pass filtered with a zero-phase filter, and then the instantaneous theta phase was extracted with a Hilbert transform. Every spike was assigned to its corresponding theta phase. Rayleigh's test for circular uniformity was applied to test the significance of phase-locking. The preferred phase and the locking strength were the argument and modulus, respectively, of the average vector of all spike events corresponding to the theta phase.

The PAC analyses were computed using direct PAC measures (Ozkurt and Schnitzler 2011) implemented in Brainstorm toolbox (Tadel et al. 2011) and defined as follows:

$$\text{PAC}(f_\varphi, f_a) = \frac{1}{\sqrt{N}} \frac{\left|\sum_{n=1}^{N} a(n) e^{i\varphi(n)}\right|}{\sqrt{\sum_{n=1}^{N} a(n)^2}}.$$

In this formula, N is the data length, n is a signal time sample, a is the signal amplitude at the high-frequency f_a, and φ is the signal phase at the low-frequency f_φ. The signal phase and amplitude were computed using the chirplet transform, following a similar methodology to that of a previous study (Canolty et al. 2006). In the current analyses, the direct PAC was calculated from all frequency pairs, with $f_\varphi \in [2, 20]$ Hz and $f_a \in [20, 150]$ Hz, with the frequency step of f_φ and f_a set to 0.75 Hz.

A modulation index (MI) was applied to compute the modulation of gamma power by the theta phase, as performed in

previous studies (Tort et al. 2008, 2009). The mean amplitude of gamma power at each phase bin (18°) was determined and then normalized to the total gamma power. Kullback–Leibler distance was calculated to quantify the phase-amplitude distribution deviating from the uniform distribution, and then divided by a constant factor to obtain the MI value.

Histological Identification

After the collection of electrophysiological data, rats were anesthetized with 3% sodium pentobarbital and a direct current of 8 mA was applied for 20 s through the electrode for electrolytic lesion. Thereafter, rats were transcardially perfused with saline followed by 4% paraformaldehyde. The brains were removed and stored in 30% sucrose and 4% paraformaldehyde solution for dehydration. Continuous frozen sections of entorhinal cortex were prepared (60 μm) and stained with Nissl's dye. The locations of the cannula and electrode were examined by visualizing the sections with a microscope.

Immunohistochemistry for c-fos Protein

Twelve rats with 1-trial recognition task training and 2 control rats were anesthetized with 3% sodium pentobarbital and perfused with saline, which was followed by a 4% paraformaldehyde perfusion. Brains were stored in phosphate-buffered solution (PBS) with 4% paraformaldehyde for one night, and then stored in 30% sucrose solution for 3 days. Brains were continuously sectioned (20-μm thick) from dorsal to ventral entorhinal cortex with a freezing microtome (CM 3050S, Leica). First, the last slice containing the drug injection site was identified, and then the next 3 slices were selected for c-fos immunohistochemistry. Slices were first washed 3 times in PBS for 5 min each, and then blocked with 5% donkey serum (Jackson ImmunoResearch) containing 1% Triton X-100 (Sigma-Aldrich) for 1.5 h at room temperature. The sections were then incubated in primary antiserum (Santa Cruz Biotechnology) for 48 h at 4°C, washed 3 times in PBS, and finally incubated in Alexa Fluor 488 donkey antirabbit IgG (H+L; Invitrogen) for 2 h. After immunostaining with DAPI and washing 3 times with PBS, the slices were mounted on slides. The number of c-fos positive neurons was analyzed by fluorescence microscopy (VS-120, Olympus), and featured images were obtained from an inverted laser scanning confocal microscope (FV1000, Olympus).

Drug Administration

Histamine, triprolidine, ranitidine, and clobenpropit were purchased from Sigma-Aldrich. All drugs were stored as stock solutions at −20°C until use. Before injection, the drugs were freshly diluted to the required concentrations in artificial cerebral spinal fluid. The stainless-steel drug cannulas were composed of a guide cannula (o.d., 0.64 mm and i.d., 0.45 mm) and a mandril. An infusion cannula (o.d., 0.41 mm and i.d., 0.25 mm) with a 200-μm protrusion from the tip to the guide cannula was used for drug administration. At the time of injection, drugs were administered by syringe pump (KD Scientific), at an infusion rate of 0.5 μL/min. The drug (1 μL) was injected on each side of the sMEC, and the injection cannula was left for 2 min in the sMEC after infusion. In the freely moving test, animals received 10 sessions of drug administration, including vehicle, histamine, triprolidine, ranitidine, clobenpropit, triprolidine plus histamine, ranitidine plus histamine, and clobenpropit plus histamine. For the spatial exploration test, 7 sessions of drug infusion were performed, including vehicle, histamine, triprolidine, ranitidine, and clobenpropit. In the spatial recognition test, 4 sessions of drugs were administered to the rats, including vehicle, triprolidine, ranitidine, and clobenpropit. The order of drug administration was selected by generation of random numbers. The animals were allowed 48 h to recover between test sessions with different drugs. The drug concentrations used in this study were histamine 30 μM, 300 μM, and 3 mM, triprolidine 10 μM, ranitidine 100 μM, and clobenpropit 10 μM, which are comparable to those used in our previous experiments (He et al. 2016) and other studies (Song et al. 2006; Yu et al. 2006; Zarrindast et al. 2010; Kraus et al. 2013).

Statistical Analysis

All values were presented as means ± SEM. Chi-square tests and partition of Chi-square tests were used for multiple comparisons (McDonald 2014). Student's paired *t*-test, one-way analysis of variance (ANOVA), two-way repeated-measures ANOVA, and Tukey's post hoc test were used for statistical analyses. Significant differences were accepted as $P < 0.05$.

Results

Histamine is Essential for Upregulating the Excitability of Putative Principal Neurons via H1Rs in the sMEC In Vivo

For drug delivery and simultaneous recording of the neural activity, we implanted the cannula into the sMEC and the electrode array was placed to the side. The electrode traces are shown in Figure 1*a*, indicating the recording sites in the sMEC. The distance from the electrodes to the tip of the drug cannula was 572 ± 136 μm. Figure 1*b*–*e* shows 2 separated units recorded from 1 electrode wire. The stability of the waveforms was illustrated by plotting the waveform shape over the recording duration (see Supplementary Fig. 1*a*).

We first investigated the role of histaminergic system in sMEC neural activities in freely moving rats. Indeed, histamine increased the firing rate of a significant proportion of neurons in the sMEC (Fig. 1*f*,*j*). We calculated the excitatory ratio, which was used to illustrate the percentage for the number of responsive neurons to the number of totally recorded neurons (Yang and Hatton 1997; Sun et al. 2015), for different levels of histamine by the formula (number of histamine-excited neurons)/(total number of neurons recorded during the test). A dose-dependent effect on the excitatory ratio was observed when the concentration of histamine was administrated from 30 μM to 3 mM (Fig. 1*j*, Chi-square test, Chi-square = 119.08 with 3 degrees of freedom, $P < 0.001$, partition of Chi-square test for multiple comparisons: $P_{\text{vehicle vs. histamine 30 μM}} < 0.01$, $P_{\text{histamine 30 μM vs. histamine 300 μM}} < 0.01$, $P_{\text{histamine 300 μM vs. histamine 3 mM}} < 0.01$; $n_{\text{vehicle}} = 154$ neurons, $n_{\text{histamine 30 μM}} = 190$ neurons, $n_{\text{histamine 300 μM}} = 194$ neurons, $n_{\text{histamine 3 mM}} = 153$ neurons). Our previous studies revealed a role for H1Rs in mediating the postsynaptic excitatory effects of histamine on sMEC principal neurons (He et al. 2016). In vivo, we consistently found that a histamine-induced increase in putative principal neuronal firing was mediated by H1Rs, because administration of the H1R antagonist triprolidine (10 μM; Fig. 1*g*), but not H2R antagonist ranitidine (100 μM; Fig. 1*h*) or H3R antagonist clobenpropit (10 μM; Fig. 1*i*), significantly decreased the firing rate of sMEC neurons (Fig. 1*k*, Chi-square test, Chi-square = 193.77 with 2 degrees of freedom, $P < 0.001$, partition of Chi-square test for multiple comparisons: $P_{\text{triprolidine vs. ranitidine}} < 0.001$,

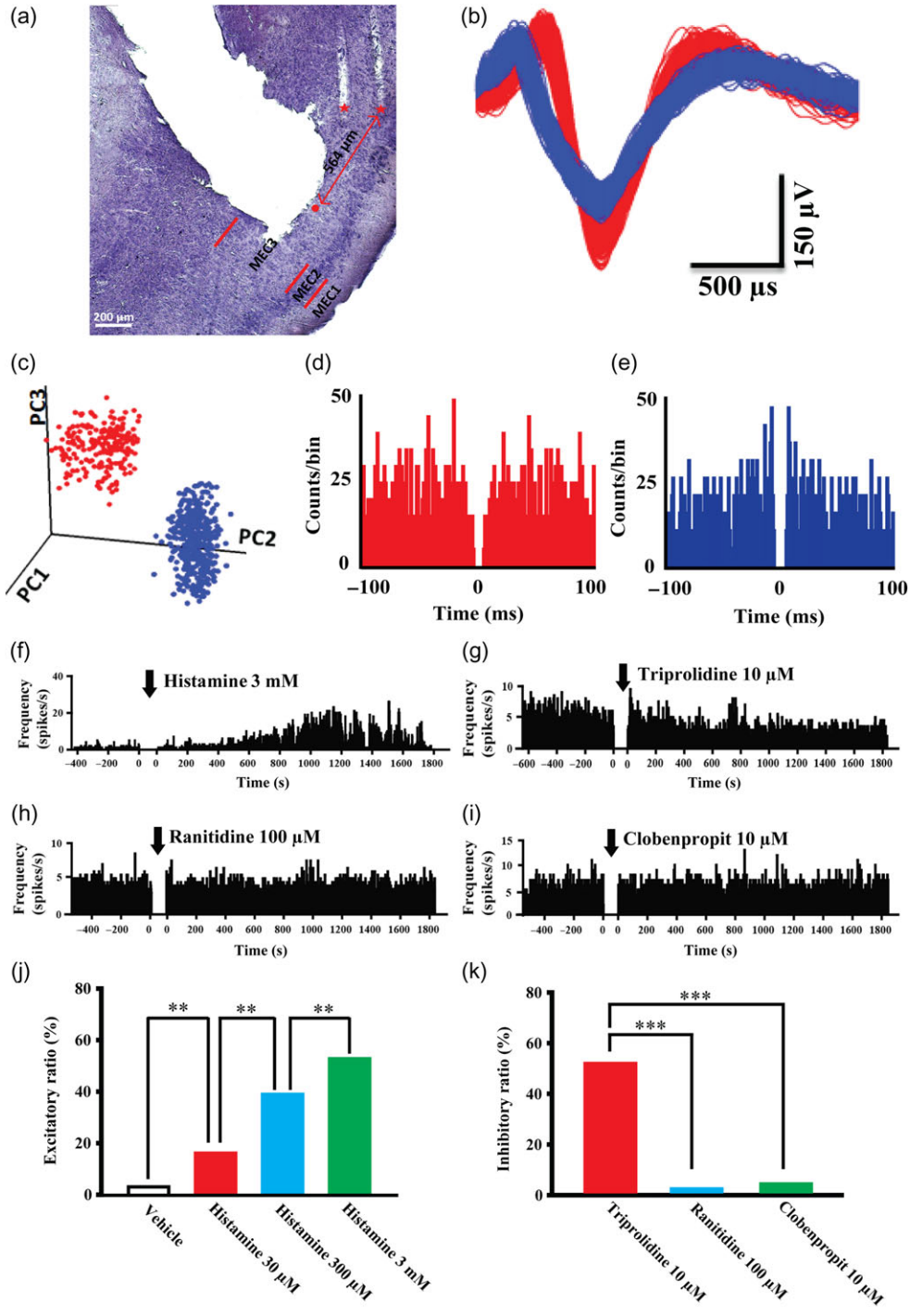

Figure 1. Histamine dose-dependently upregulates the neuronal excitability via activation of type 1 histamine receptors (H1Rs) in the sMEC. (*a*) Nissl's staining showing the recording sites (red asterisk) and implantation of drug cannula (red dot) in the sMEC. Representative waveforms (*b*), PCs (*c*), and autocorrelograms (*d*,*e*) of 2 separated units recorded from a single wire. (*f*) Histamine (3 mM) increased the firing rate of putative principal neurons in the sMEC. Arrow indicates the administration of histamine. (*g*) The antagonist of H1Rs (triprolidine, 10 μM) inhibited excitability of putative principal neurons with a decreased firing rate. (*h*,*i*) The antagonist of H2Rs (ranitidine, 100 μM, *h*) or H3Rs (clobenpropit, 10 μM, *i*) has no effects on the firing rate of putative principal neurons. (*j*) Histamine at concentrations from 30 μM to 3 mM dose-dependently increased the excitatory ratio of putative principal neurons. (*k*) Inhibitory ratio of triprolidine (10 μM), ranitidine (100 μM), and clobenpropit (10 μM) on putative principal neuronal firing in the sMEC. **P < 0.01, ***P < 0.001.

$P_{\text{triprolidine vs. clobenpropit}} < 0.001$, $P_{\text{ranitidine vs. clobenpropit}} > 0.05$; $n_{\text{triprolidine}} = 192$ neurons, $n_{\text{ranitidine}} = 189$ neurons, $n_{\text{clobenpropit}} = 196$ neurons). To further confirm the receptor mechanisms, we investigated the effects of histamine in the presence of the receptor antagonists triprolidine, ranitidine, or clobenpropit. Similarly, triprolidine at 10 μM (see Supplementary Fig. 1*b*), but not ranitidine (100 μM; see Supplementary Fig. 1*c*) or clobenpropit (10 μM; see Supplementary Fig. 1*d*), significantly blocked the histamine-mediated elevation of firing rate and the response ratio of putative principal neurons (see Supplementary Fig. 1*e*;

Chi-square test, Chi-square = 126.19 with 4 degrees of freedom, $P < 0.001$; partition of Chi-square test for multiple comparisons: $P_{\text{vehicle vs. histamine}} < 0.001$, $P_{\text{histamine vs. (triprolidine + histamine)}} < 0.001$; $n_{\text{vehicle}} = 154$ neurons, $n_{\text{histamine}} = 153$ neurons, $n_{\text{triprolidine+histamine}} = 65$ neurons). No significant difference was observed between groups for the response ratio of histamine, histamine plus ranitidine, or histamine plus clobenpropit (see Supplementary Fig. 1*e*; Chi-square test, Chi-square = 2.175 with 2 degrees of freedom, $P > 0.05$; $n_{\text{histamine}} = 153$ neurons, $n_{\text{ranitidine+histamine}} = 59$ neurons, $n_{\text{clobenpropit+histamine}} = 54$ neurons). These results demonstrated that, in vivo, activation of H1Rs increases the neuronal excitability of putative principal neurons in the sMEC.

H1R and H3R Activation Mediates Histamine-Induced Increases of Theta and High Gamma Power in the sMEC In Vivo

We previously reported that in addition to the H1R-mediated postsynaptic effects, histamine activated the presynaptic H3Rs and inhibited gamma-aminobutyric acid (GABA) release in the sMEC, which was observed as decreased mini-inhibitory postsynaptic currents (mIPSCs) (He et al. 2016). The excitatory postsynaptic currents (EPSCs) or IPSCs were contributors of local oscillatory activities, especially the theta and gamma oscillations. In the analysis of LFP, we found that histamine significantly increased the power of theta (Fig. 2*a*) and gamma oscillations (Fig. 2*b*,*c*) in the sMEC when rats were freely moving in the open field. We calculated the PSD for different frequency bands after injection of vehicle (Fig. 2*d*) and histamine (Fig. 2*g*). Statistical analyses showed that histamine at 30 μM increased high gamma power and reduced delta power, with no effects on the theta and low gamma oscillations (Fig. 2*f*, paired *t*-test, $P_{\text{delta}} < 0.01$, $P_{\text{theta}} > 0.05$, $P_{\text{low gamma}} > 0.05$, $P_{\text{high gamma}} < 0.001$, $n = 11$ rats). Both theta and high gamma power were increased after administration of 300 μM and 3 mM histamine (Fig. 2*g*,*h*,*i*, paired *t*-test, 300 μM: $P_{\text{delta}} < 0.001$, $P_{\text{theta}} < 0.01$, $P_{\text{low gamma}} > 0.05$, $P_{\text{high gamma}} < 0.001$, $n = 11$ rats; 3 mM: $P_{\text{delta}} < 0.001$, $P_{\text{theta}} < 0.001$, $P_{\text{high gamma}} < 0.001$, $n = 11$ rats). Moreover, histamine at 3 mM enhanced the power of low gamma (Fig. 2*i*, paired *t*-test, $P_{\text{low gamma}} < 0.001$, $n = 11$ rats). In the next step, we explored the roles of H1Rs and H3Rs in sMEC neural oscillatory activities. Both H1Rs and H3Rs were involved in modulating local theta and high gamma oscillations (Fig. 2*j*–*l*). The administration of triprolidine (10 μM, *j*) or clobenpropit (10 μM, *l*) significantly decreased theta and high gamma power, while infusion of ranitidine (100 μM, *k*) did not change the local power of theta and high gamma in the sMEC (Fig. 2*m*–*o*, paired *t*-test, triprolidine, $P_{\text{delta}} < 0.001$, $P_{\text{theta}} < 0.001$, $P_{\text{beta}} < 0.01$, $P_{\text{low gamma}} < 0.05$, $P_{\text{high gamma}} < 0.001$, $n = 11$ rats; ranitidine, all comparisons $P > 0.05$, $n = 11$ rats; Clobenpropit, $P_{\text{delta}} < 0.001$, $P_{\text{theta}} < 0.001$, $P_{\text{high gamma}} < 0.001$, $n = 11$ rats). Together, our results indicate roles for H1Rs and H3Rs in the histaminergic modulation of theta and high gamma power in the sMEC.

Histaminergic Input Does Not Affect the Encoding of Gridness or Borderness

Because histamine plays an important role in enhancing neuronal excitability, local theta, and high gamma oscillations, it remains largely unknown whether the histaminergic system can influence the neuronal spatial encoding in the sMEC. During the test of spatial exploration, scattered food was randomly spread in the open field. Rats were motivated by the food to explore the entire open field. Our data here showed that neither histamine (300 μM, 3 mM; Fig. 3*a*,*b*, see Supplementary Fig. 2*a*,*d*–*i*) nor its receptor antagonists, including triprolidine (10 μM; Fig. 3*a*,*b*), ranitidine (100 μM; see Supplementary Fig. 2*b*,*d*–*i*), or clobenpropit (10 μM; see Supplementary Fig. 2*c*,*d*–*i*), affected the encoding of gridness, including the gridness score, average rate, peak rate, information rate, sparsity, or mean field size of grid cells (Fig. 3b, see Supplementary Fig. 2*d*–*l*; paired *t*-test, all comparisons $P > 0.05$, $n_{\text{vehicle}} = 12$ neurons, $n_{\text{histamine 3 mM}} = 17$ neurons, $n_{\text{histamine 300 μM}} = 13$ neurons, $n_{\text{triprolidine}} = 14$ neurons, $n_{\text{ranitidine}} = 16$ neurons, $n_{\text{clobenpropit}} = 15$ neurons). Moreover, there was no statistically significant difference in the borderness score between baseline and vehicle (Fig. 3*c*,*d*; paired *t*-test, $P > 0.05$, $n_{\text{vehicle}} = 13$ neurons). Infusion of histamine (300 μM) or triprolidine (10 μM) had no effect on the borderness score (Fig. 3*c*,*d*; paired *t*-test, 2 comparisons $P > 0.05$, $n_{\text{histamine}} = 14$ neurons, $n_{\text{triprolidine}} = 13$ neurons).

Theta Phase-Locking of Putative Principal Neurons and Theta–High Gamma Coupling in the sMEC are Enhanced by Histamine During Spatial Exploration

During spatial exploration, theta oscillations were found to be the temporal code for local calculation in the entorhinal–hippocampal circuits (Mizuseki et al. 2009). The typical encoding patterns of information in the sMEC were the followings: theta phase-locking; the firing of neurons was concentrated at a relatively fixed theta phase (Mizuseki et al. 2009; Tang et al. 2014), and theta–gamma coupling; the maximal gamma power was coupled tightly with the theta cycle (Chrobak and Buzsaki 1998; Colgin et al. 2009). Although the histaminergic system did not influence the encoding of gridness and borderness, we speculate that it probably plays a role in regulating the theta phase-locking and theta–gamma coupling in the sMEC. Surprisingly, unlike the vehicle (Fig. 4*a*–*c*; paired *t*-test, $P_{\text{preferred phase}} > 0.05$, $P_{\text{locking strength}} > 0.05$, $n = 132$ neurons), histamine (3 mM) increased the strength of theta-modulated spiking of putative principal neurons (Fig. 4*d*,*f*; paired *t*-test, $P < 0.001$, $n = 112$ neurons), with no effect on the preferred locking phase (Fig. 4*d*,*e*; paired *t*-test, $P > 0.05$, $n = 112$ neurons). Administration of triprolidine (10 μM; Fig. 4*g*,*i*), but not ranitidine (100 μM; Fig. 4*j*,*l*) or clobenpropit (10 μM; Fig. 4*m*,*o*), decreased the locking strength (paired *t*-test, $P_{\text{triprolidine}} < 0.001$, $P_{\text{ranitidine}} > 0.05$, $P_{\text{clobenpropit}} > 0.05$, $n_{\text{triprolidine}} = 119$ neurons, $n_{\text{ranitidine}} = 136$ neurons, $n_{\text{clobenpropit}} = 142$ neurons), suggesting a role for H1Rs in histamine-induced enhancement of theta phase-locking. Neither triprolidine (Fig. 4*g*,*h*) nor ranitidine (Fig. 4*j*,*k*), nor clobenpropit (Fig. 4*m*,*n*) influenced the preferred phase of theta locking (paired *t*-test, all comparisons $P > 0.05$, $n_{\text{triprolidine}} = 119$ neurons, $n_{\text{ranitidine}} = 136$ neurons, $n_{\text{clobenpropit}} = 142$ neurons). Furthermore, H1R antagonists (see Supplementary Fig. 3*a*), but not the H2R or H3R antagonists (see Supplementary Fig. 3*b*,*c*), significantly inhibited the histamine-elicited enhancement of the theta phase-locking strength of putative principal neurons (see Supplementary Fig. 3*g*–*l*; paired *t*-test, $P_{\text{triprolidine vs. (triprolidine+histamine)}} > 0.05$, $P_{\text{ranitidine vs. (ranitidine+histamine)}} < 0.001$, $P_{\text{clobenpropit vs. (clobenpropit+histamine)}} < 0.001$, $n_{\text{triprolidine}} = 129$ neurons, $n_{\text{ranitidine}} = 101$ neurons, $n_{\text{clobenpropit}} = 99$ neurons), with no effect on preferred phase (see Supplementary Fig. 3*d*–*f*; paired *t*-test, all comparisons $P > 0.05$).

During spatial exploration, the amplitude of low gamma (25–48 Hz) and high gamma (60–120 Hz) was locked to the theta (4–12 Hz) phase (Fig. 5*a*–*e*). Interestingly, histamine (3 mM) specifically enhanced the coupling between theta phase and high gamma power (Fig. 5*c*,*e*,*g*; paired *t*-test, $P < 0.001$, $n = 11$ rats). Injection of histamine has no effect on the theta–low gamma

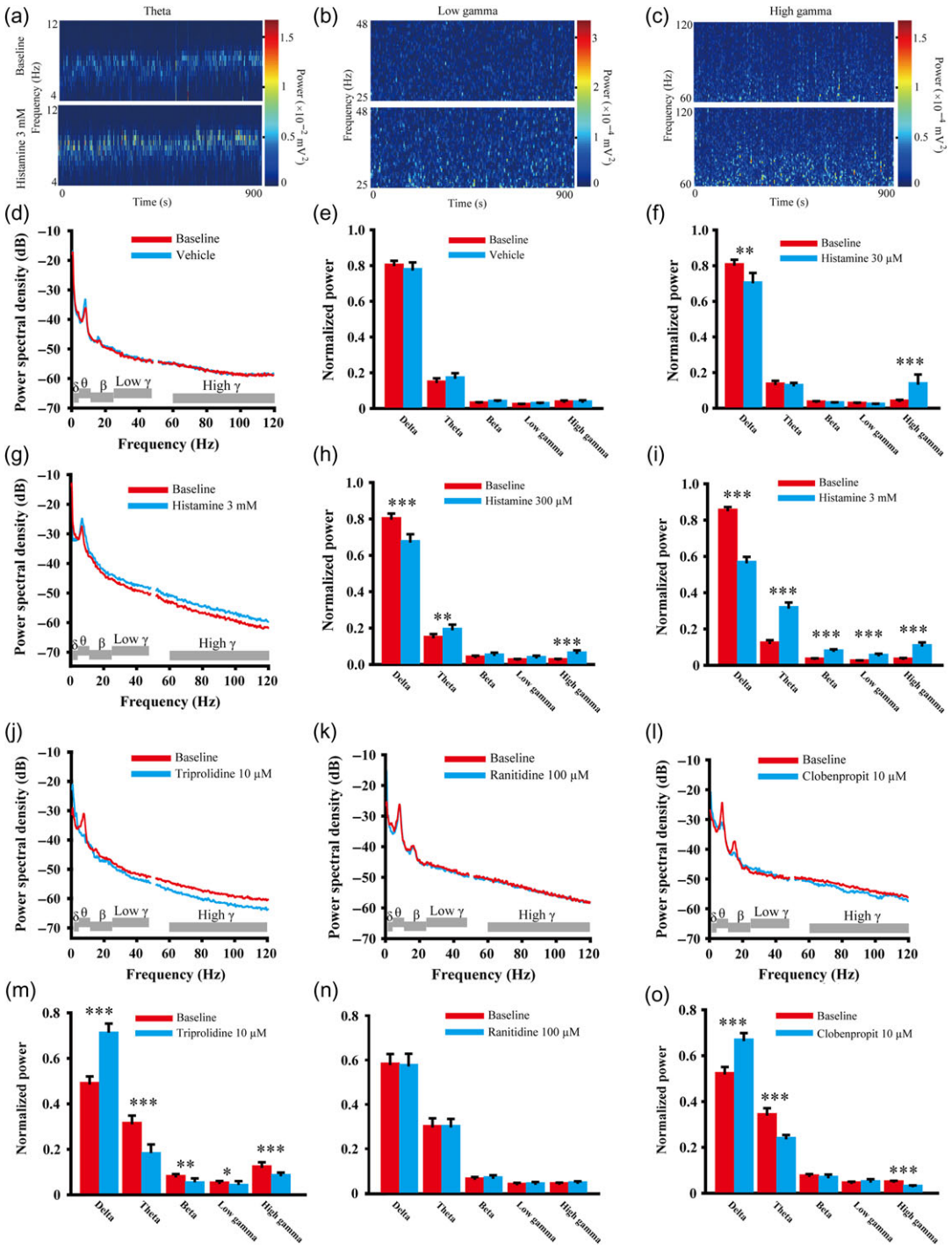

Figure 2. H1Rs and H3Rs are involved in histamine-induced increase of local theta and high gamma power. The spectrogram of theta (*a*), low gamma (*b*), and high gamma (*c*) oscillatory power in the sMEC during baseline (top panel) and histamine (3 mM, bottom panel) sessions, when rats were freely exploring the open field. Traces of PSD during baseline and vehicle (*d*) or histamine (3 mM, *g*) sessions. Statistical results of the effects of vehicle (*e*) or histamine at 30 μM (*f*), 300 μM (*h*), or 3 mM (*i*) on normalized delta, theta, beta, low gamma, and high gamma power in the sMEC. Traces of PSD during baseline recording and administration of histamine receptor antagonists triprolidine (10 μM, *j*), ranitidine (100 μM, *k*) and clobenpropit (10 μM, *l*). Both H1R antagonist triprolidine (*m*) and H3R antagonist clobenpropit (*o*) reduced the theta and the high gamma power in th sMEC while H2R antagonist ranitidine (*n*) has no effects. *$P < 0.05$, **$P < 0.01$, ***$P < 0.001$.

coupling (Fig. 5c,*d*,*f*; paired *t*-test, $P > 0.05$, $n = 11$ rats). In the investigation of receptor mechanisms underlying the enhanced theta–high gamma coupling, we found that the MI was decreased in the presence of either triprolidine (10 μM; Fig. 5*g*; paired *t*-test, $P < 0.001$, $n = 11$ rats) or clobenpropit (10 μM; Fig. 5*g*, paired *t*-test, $P < 0.05$, $n = 11$ rats), but not ranitidine (100 μM; Fig. 5*g*, paired *t*-test, $P > 0.05$, $n = 11$ rats), indicating that both H1Rs and H3Rs are involved in modulation of histamine-elicited enhancement of theta–high gamma coupling in the sMEC.

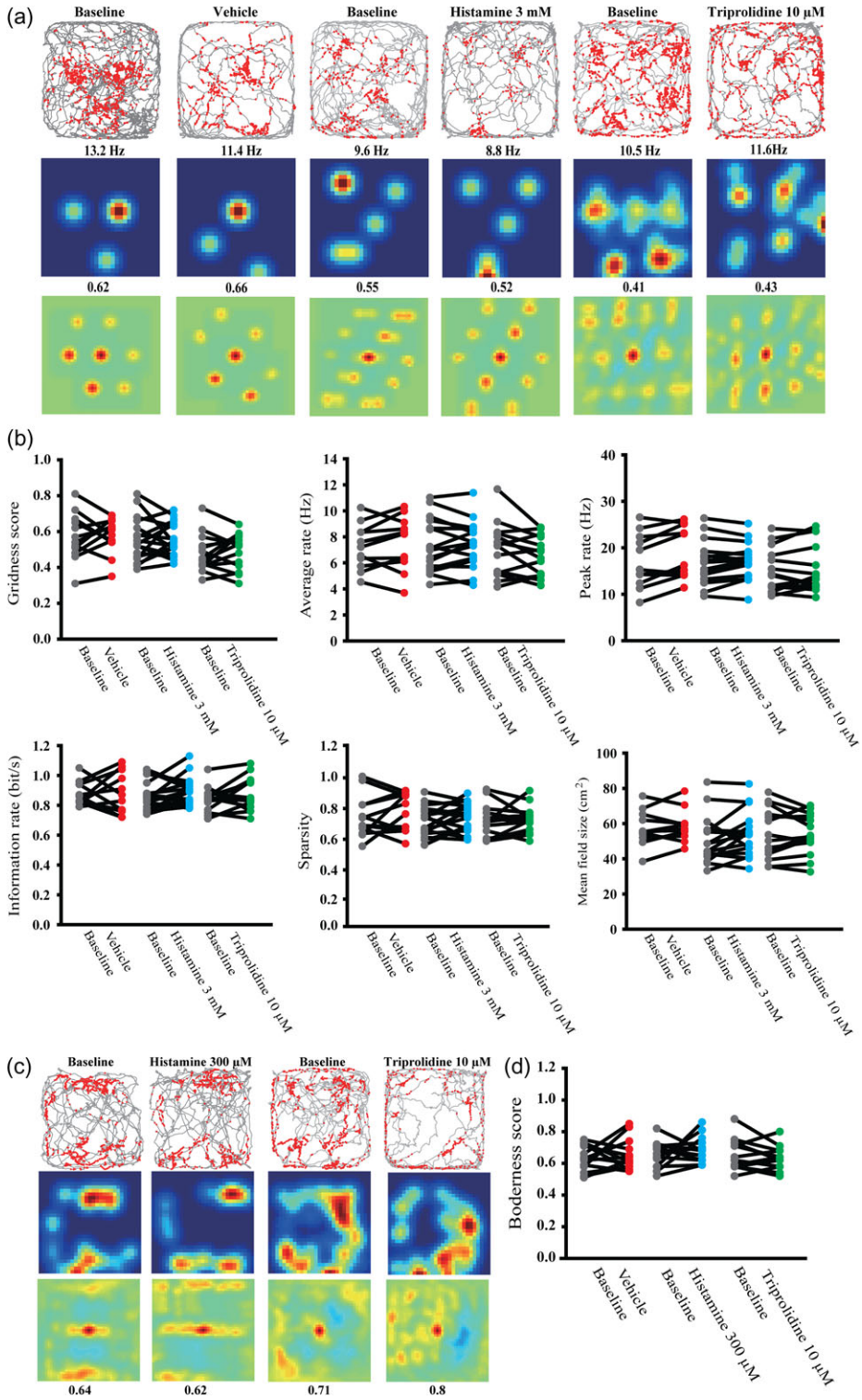

Figure 3. Histaminergic input does not affect the encoding of grid cells and border cells. (*a*) Representative spike (red dots)–trajectory (gray lines) plot (upper row), firing rate map (middle row), and spatial autocorrelation map (bottom row) of grid cells during baseline and vehicle, histamine (3 mM), and H1R antagonist triprolidine (10 μM) sessions. The corresponding maximal firing rate and gridness score were marked above the maps. (*b*) Statistics of gridness score, average firing rate, peak rate, information rate, sparsity, and mean field size of grid cells in baseline and vehicle, histamine (3 mM), and triprolidine (10 μM) groups. (*c*) Spike–trajectory plot, rate map, and autocorrelation map of representative border cells in the sMEC during baseline and histamine (300 μM), or triprolidine (10 μM) sessions. (*d*) Histamine (300 μM) or H1R antagonist triprolidine (10 μM) did not influence the value of borderness score.

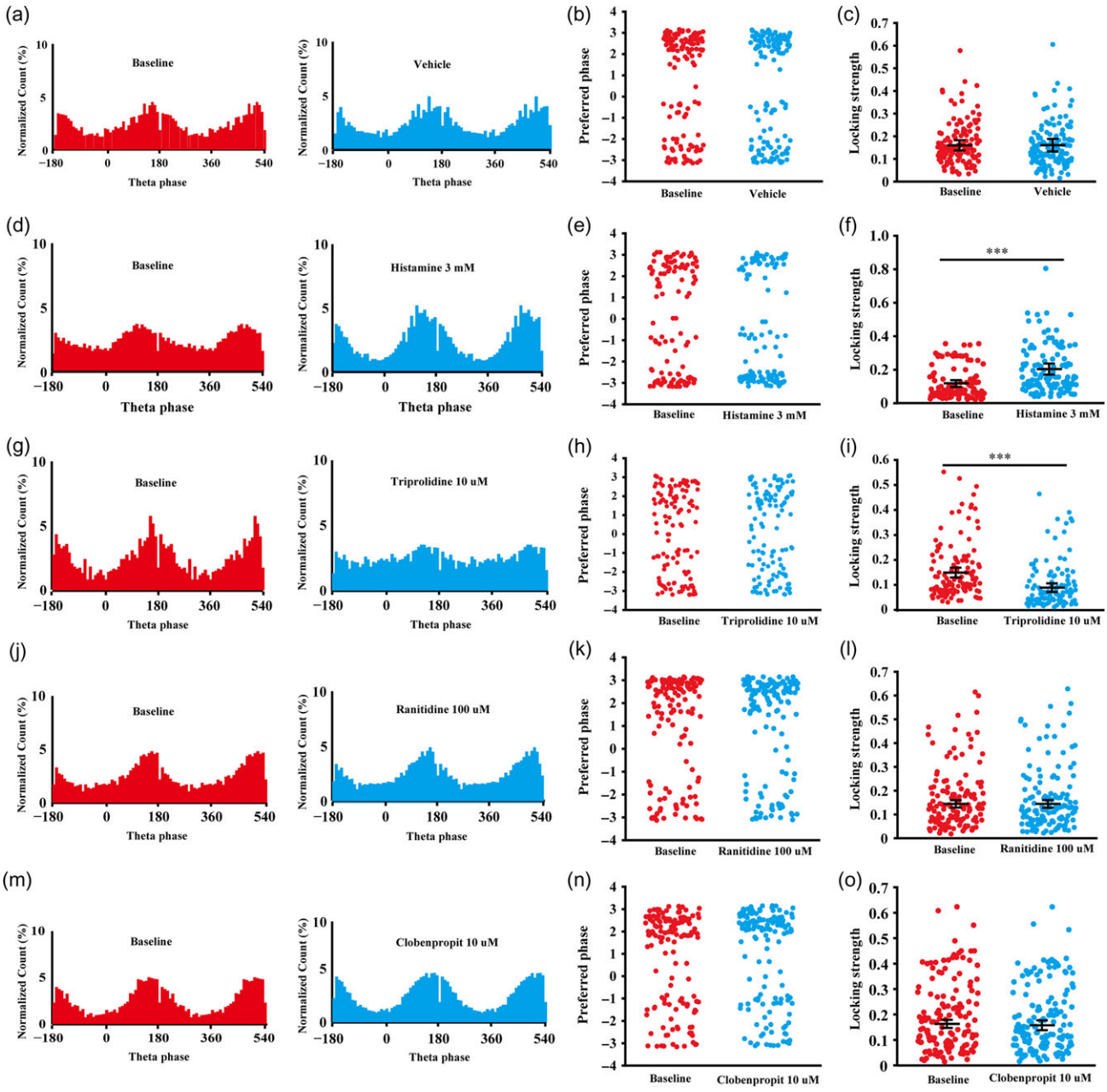

Figure 4. Histamine enhances the strength, but not the preferred phase, of theta phase-locking in the sMEC. Examples of theta phase histogram of spikes in baseline and vehicle (*a*) or histamine (3 mM) sessions (*d*). Vehicle (*b*) or histamine (3 mM, *e*) did not influence the preferred phase of theta locking. Histamine (3 mM, *f*), but not vehicle (*c*), significantly increased the locking strength of putative principal neurons at theta phase. Plots of theta phase-modulated spiking of putative principal neurons in the sMEC during baseline, triprolidine (10 μM, *g*), ranitidine (100 μM, *j*), and clobenpropit (10 μM, *m*) sessions. Dot plots of preferred locking phase of each putative principal neuron in baseline, triprolidine (*h*), ranitidine (*k*), and clobenpropit (*n*) groups. The H1R antagonist triprolidine (*i*), but not H2R antagonist ranitidine (*l*) or H3R antagonist clobenpropit (*o*), reduced the locking strength of theta-modulated spiking in the sMEC. ***$P < 0.001$.

Histaminergic System in the sMEC Regulates Spatial Recognition Performance

Recent evidence highlights the essential role of the sMEC in spatial recognition (Van Cauter et al. 2013; Reagh and Yassa 2014). We demonstrated that histamine enhances the theta modulation of spiking and high gamma oscillations in the sMEC. Whether these effects contribute to sMEC-related functions should be further clarified. We applied 2 similar paradigms to investigate the role of histamine in spatial recognition, a 1-trial recognition task and an object exploration task (Fig. 6*a*, see Materials and Methods). Rats had to recognize either a changed spatial configuration or a novel object. Blocking of the histaminergic system in the sMEC did not influence the cumulative distance or the speed of rats during these 2 spatial recognition tasks (Fig. 6*b*,*c*, and see Supplementary Fig. 4*a*–*d*; 2-way repeated-measures of ANOVA, distance: habituation trial, group effect, $F_{3,167} = 1.003$, $P > 0.05$, spatial changed trial, group effect, $F_{3,167} = 1.153$, $P > 0.05$, interaction effect, $P > 0.05$, $n = 6$ rats; speed: habituation trial, group effect, $F_{3,143} = 0.755$, $P > 0.05$, spatial changed trial, group effect, $F_{3,143} = 1.074$,

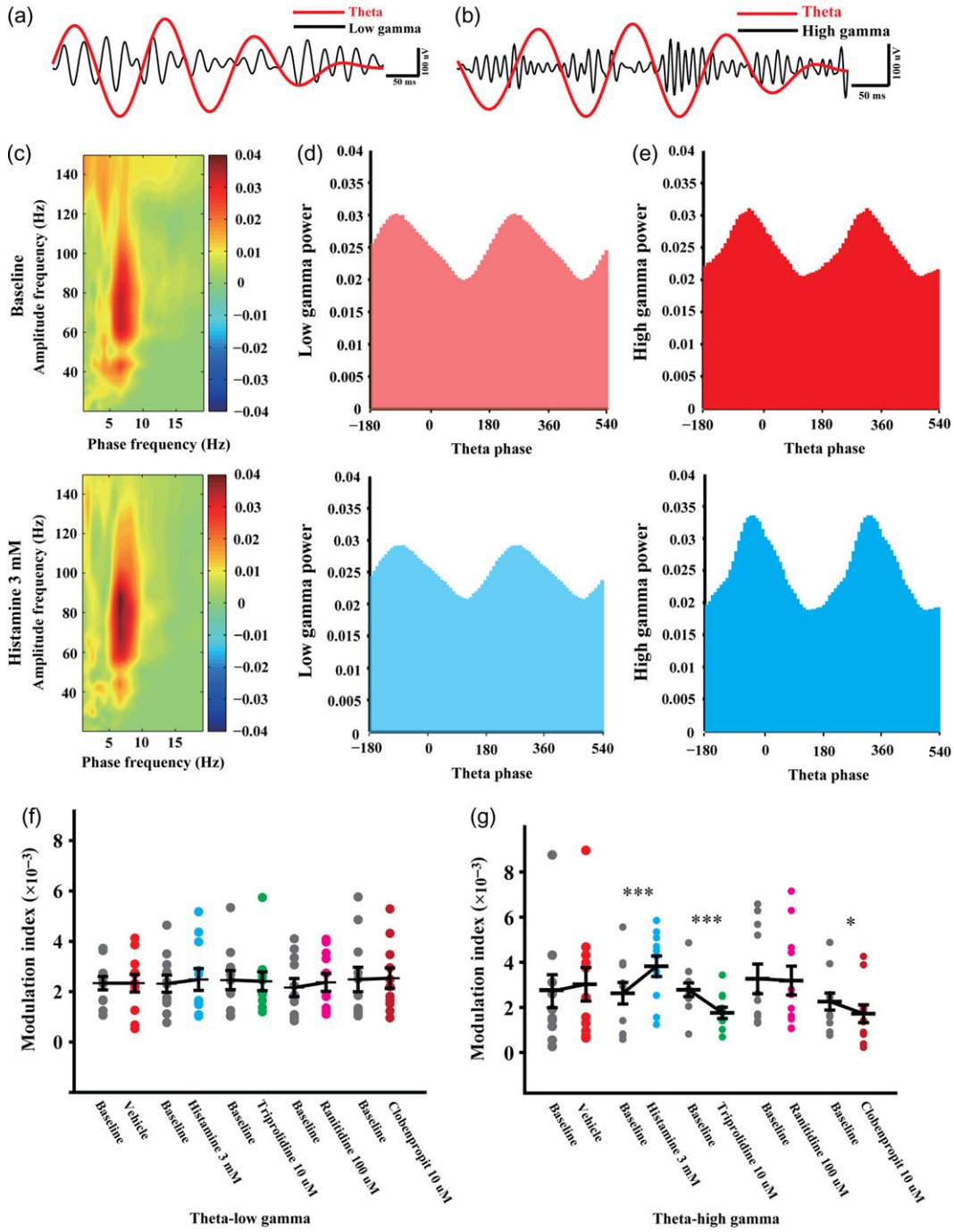

Figure 5. Histamine increases theta–high gamma coupling in the sMEC through activation of H1Rs and H3Rs in the sMEC during spatial exploration. Raw traces for overlay of filtered theta and low gamma (*a*), theta and high gamma (*b*) oscillations during the baseline session. (*c*) Examples of phase-amplitude comodulograms in the sMEC during baseline (top panel) and histamine (3 mM, bottom panel) sessions. Representative histograms of normalized low gamma (*d*) and high gamma (*e*) amplitude as a function of theta phase during baseline (top panel) and histamine (bottom panel) sessions. (*f*) Histamine and its receptor antagonists have no statistically significant effects on the MI of theta–low gamma coupling. (*g*) Histamine increased, while H1R antagonist triprolidine (10 μM) and H3R antagonist clobenpropit (10 μM) decreased, the MI of theta–high gamma coupling in the sMEC. The H2R antagonist ranitidine (100 μM) did not influence the theta phase nested high gamma power. *$P < 0.05$, ***$P < 0.001$.

$P > 0.05$, interaction effect, $P > 0.05$, $n = 6$ rats). A dramatically decreased re-exploration score of the displaced object was observed after administration of the H1R antagonist triprolidine (10 μM), but not the H2R antagonist ranitidine (100 μM), or the H3R antagonist clobenpropit (10 μM), suggesting that the histaminergic system in the sMEC is essential for spatial recognition (Fig. 6*d*; two-way repeated-measures of ANOVA, effects of drugs, $F_{3,47} = 3.756$, $P < 0.001$; effects of displaced object and nondisplaced objects, $P < 0.001$; interaction effect, $P > 0.05$; Tukey's test for multiple comparisons: vehicle, $P_{\text{displaced vs. nondisplaced}} < 0.001$, triprolidine, $P_{\text{displaced vs. nondisplaced}} > 0.05$, ranitidine, $P_{\text{displaced vs. nondisplaced}} < 0.001$, clobenpropit, $P_{\text{displaced vs. nondisplaced}} < 0.001$;

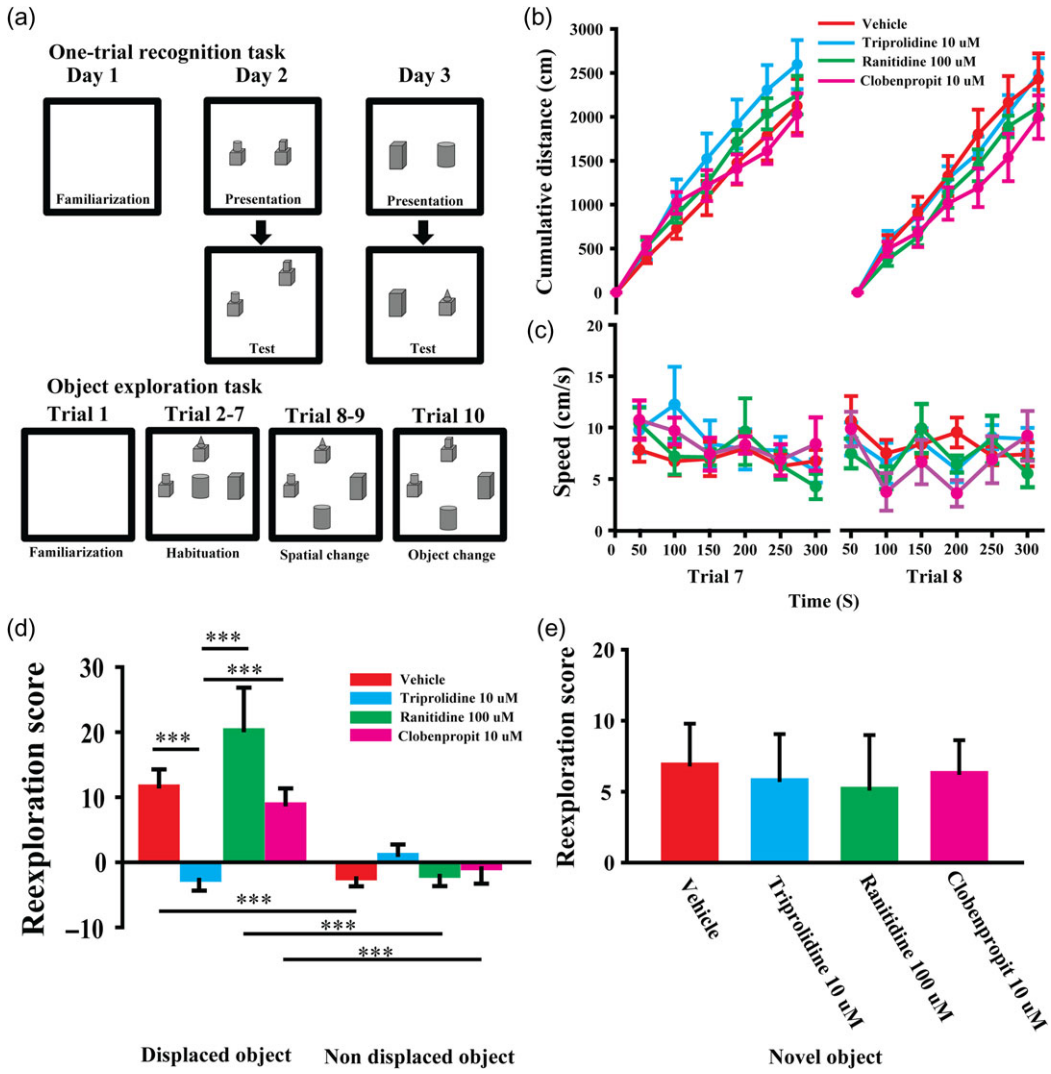

Figure 6. Histaminergic system in the sMEC contributes to spatial recognition. (*a*) Paradigms of 1-trial recognition task (top panel) and object exploration task (bottom panel). During the object exploration task, the cumulative distance (*b*) and the speed (*c*) were not different between trial 7 (left column) and trial 8 (right column) during the vehicle, triprolidine (10 μM), ranitidine (100 μM), and clobenpropit (10 μM) groups. (*d*) H1R antagonist triprolidine, but not H2R antagonist ranitidine or H3R antagonist clobenpropit, significantly reduced the re-exploration score of changed spatial configuration, with no statistical differences between the displaced object and the nondisplaced object. (*e*) As for the exploration for novel object, inhibition of histamine receptors by its antagonists did not affect the re-exploration score during the 10th trial. ***$P < 0.001$.

displaced object, $P_{\text{vehicle vs. triprolidine}} < 0.001$, $P_{\text{triproline vs. ranitidine}} < 0.001$, $P_{\text{triprolidine vs. clobenpropit}} < 0.001$, nondisplaced object, all comparisons, $P > 0.05$, $n = 6$ rats; see Supplementary Fig. 4*e*; 1-way ANOVA, $P < 0.05$, Tukey's test for multiple comparisons: $P_{\text{vehicle vs. triprolidine}} < 0.05$, $P_{\text{triproline vs. ranitidine}} < 0.05$, $P_{\text{triprolidine vs. clobenpropit}} < 0.05$, $n = 6$ rats). To further confirm that neuronal activities in the sMEC were involved in histamine-modulated spatial recognition, we analyzed the c-fos expression after the 1-trial recognition test. Compared with the baseline (see Supplementary Fig. 5*a*), c-fos expression was significantly increased after training in the spatial recognition task (see Supplementary Fig. 5*b*). Blocking of H1Rs, but not H2Rs or H3Rs, inhibited the increase of c-fos expression after training (see Supplementary Fig. 5*c–f*; 1-way ANOVA, $P < 0.001$, Tukey's test for multiple comparisons: $P_{\text{baseline vs. vehicle}} < 0.001$, $P_{\text{baseline vs. ranitidine}} < 0.001$, $P_{\text{baseline vs. clobenpropit}} < 0.001$, $P_{\text{triprolidine vs. vehicle}} < 0.001$, $P_{\text{triprolidine vs. ranitidine}} < 0.001$, $P_{\text{triprolidine vs. clobenpropit}} < 0.001$, baseline group: $n = 8$ slices from 2 rats, all other groups: $n = 9$ slices from 3 rats). However, disruption of the histaminergic system did not affect the performance of rats in the recognition of novel objects (Fig. 6*e* and see Supplementary Fig. 4*f*; 1-way ANOVA, all comparisons $P > 0.05$, $n = 6$ rats), which is consistent with previous studies showing the different roles of medial and lateral entorhinal cortex in spatial recognition and object recognition, respectively (Van Cauter et al. 2013; Morrissey and Takehara-Nishiuchi 2014). These data revealed that the histaminergic system is essential for the successful execution of sMEC-related spatial functions at behavioral levels.

Histamine-Modulated Spatial Recognition is Closely Linked to Theta Phase-Locking and Theta–High Gamma Coupling

To clarify whether the histamine-induced theta modulation of spiking and high gamma oscillations in the sMEC are correlated with spatial recognition performance, we investigated the theta phase-locking of putative principal neurons and theta–high

gamma coupling in the sMEC during behavioral tests. Interestingly, compared with the habituation session, a significant portion of putative principal neurons in the sMEC showed an increased theta phase-locking strength, but not the preferred phase, during the exploration of changed spatial configuration (Fig. 7*a*,*e*,*i*,*m*; paired *t*-test, preferred phase: $P > 0.05$, locking strength: $P < 0.001$, $n = 62$ neurons; see Supplementary Fig. 6*a*,*e*,*i*; paired *t*-test, preferred phase: $P > 0.05$, locking strength: $P < 0.001$, $n = 59$ neurons). Blocking the H1Rs significantly decreased the strength of theta phase-locking during habituation and the elevation of the locking strength during spatial recognition (Fig. 7*b*,*f*,*j*,*n*; paired *t*-test, 2 comparisons, $P > 0.05$, $n = 85$ neurons; see Supplementary Fig. 6*b*,*f*,*j*; paired *t*-test, 2 comparisons, $P > 0.05$, $n = 53$ neurons). In line with the aforementioned behavioral results, the microinjection of H2R or H3R antagonists has no effects on the elevation of theta phase-locking of putative principal neurons during spatial recognition (Fig. 7*c*,*d*,*g*,*h*,*k*,*l*,*o*,*p*; paired *t*-test, preferred phase: 2 comparisons $P > 0.05$, locking strength: 2 comparisons, $P < 0.001$, $n_{ranitidine} = 61$ neurons, $n_{clobenpropit} = 68$ neurons; see Supplementary Fig. 6*c*,*d*,*g*,*h*,*k*,*l*; paired *t*-test, preferred phase: 2 comparisons $P > 0.05$, locking strength: 2 comparisons, $P < 0.001$, $n_{ranitidine} = 48$ neurons, $n_{clobenpropit} = 55$ neurons).

Similar to the increased theta phase-locking strength, we found that the theta–high gamma coupling was also elevated during spatial recognition. The elevated theta–high gamma coupling was blocked by the H1R antagonists, rather than the H2R or H3R antagonists (Fig. 8*a*,*b*; 2-way repeated-measures of ANOVA, effect of habituation-spatial-change, $F_{1,47} = 124.57$, $P < 0.001$, effects of drugs, $F_{3,47} = 152.46$, $P < 0.001$, interaction effect, $P > 0.05$; Tukey's test for multiple comparisons: vehicle, $P_{habituation\ vs.\ spatial\text{-}change} < 0.001$, triprolidine, $P_{habituation\ vs.\ spatial\text{-}change} > 0.05$, ranitidine, $P_{habituation\ vs.\ spatial\text{-}change} < 0.001$, clobenpropit, $P_{habituation\ vs.\ spatial\text{-}change} < 0.001$; habituation, $P_{vehicle\ vs.\ triprolidine} < 0.01$, $P_{vehicle\ vs.\ clobenpropit} < 0.05$, $P_{triprolidine\ vs.\ ranitidine} < 0.01$, $P_{ranitidine\ vs.\ clobenpropit} < 0.05$; spatial-change, $P_{vehicle\ vs.\ triprolidine} < 0.001$, $P_{triprolidine\ vs.\ ranitidine} < 0.001$, $P_{triprolidine\ vs.\ clobenpropit} < 0.01$, $n = 6$ rats; see Supplementary Fig. 7*a*–*c*; effect of drugs, $F_{3,47} = 84.2$, $P < 0.001$, effect of presentation-test, $F_{1,47} = 58.87$, $P < 0.05$, interaction effect, $P > 0.05$, Tukey's test for multiple comparisons: vehicle, $P_{presentation\ vs.\ test} < 0.01$, triprolidine, $P_{presentation\ vs.\ test} > 0.05$,

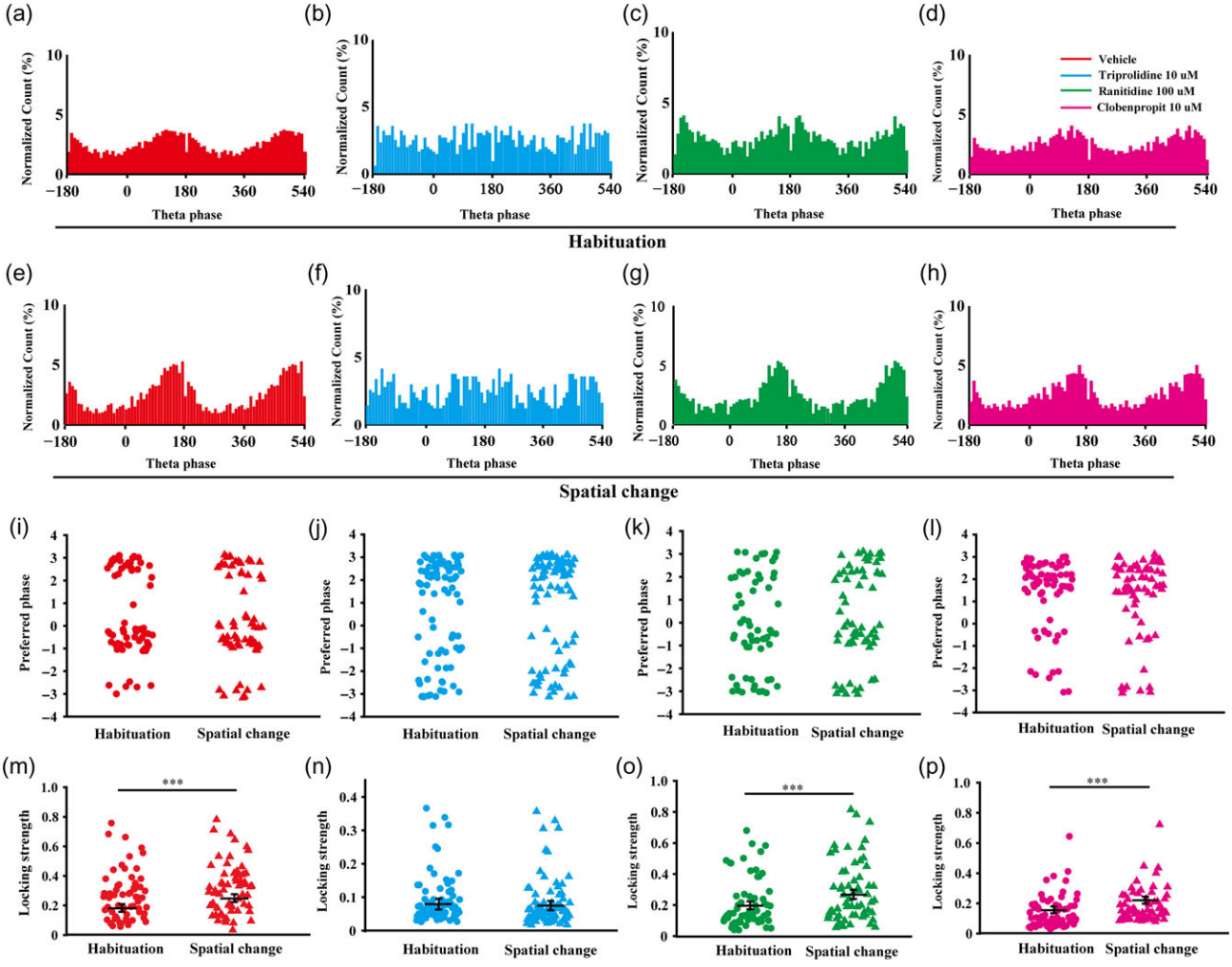

Figure 7. Histamine-modulated theta phase-locking of putative principal neurons is consistent with spatial recognition performance. Examples of histograms for neuronal spike counts as a function of theta phase during the habituation trial (top panel) and spatial-change trial (bottom panel) in the vehicle (*a*,*e*), triprolidine (10 μM, *b*,*f*), ranitidine (100 μM, *c*,*g*), and clobenpropit (10 μM, *d*,*h*) groups. Vehicle (*i*), triprolidine (*j*), ranitidine (*k*), and clobenpropit (*l*) did not influence the preferred phase of theta phase-locking in the habituation trial and changed spatial configuration trial. Dot plots showing the theta locking strength for each neuron in the sMEC during habituation and spatial-change trials in vehicle (*m*), triprolidine (*n*), ranitidine (*o*), and clobenpropit (*p*) groups. ***$P < 0.001$.

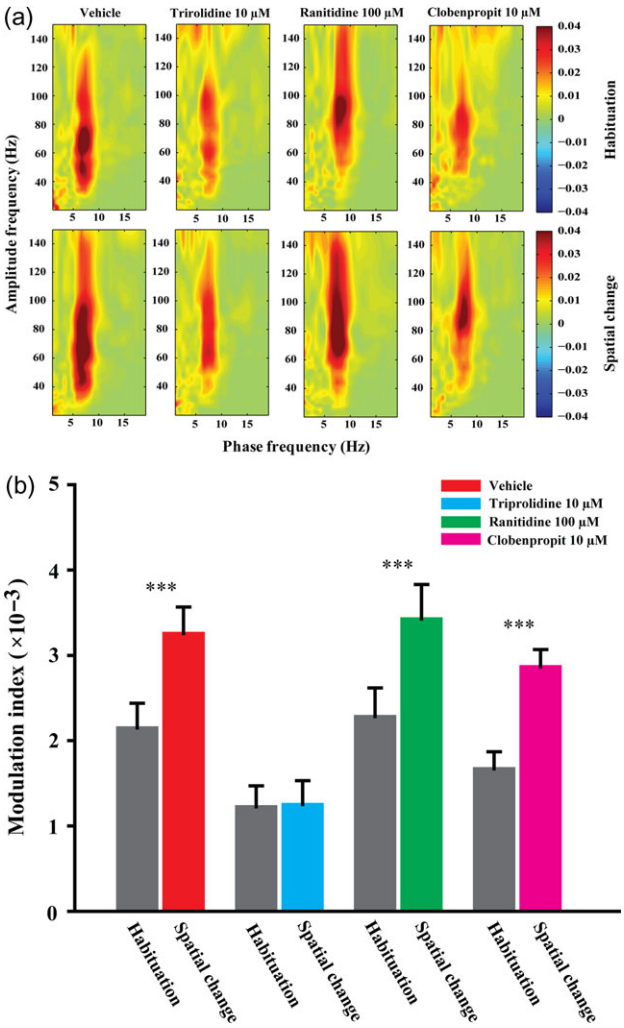

Figure 8. Theta–high gamma coupling strength is correlated with histaminergic modulation of spatial recognition in the sMEC. (*a*) Representatives of phase-amplitude comodulograms during the habituation trial (top row) and spatial-change trial (bottom row) in vehicle, triprolidine (10 μM), ranitidine (100 μM), and clobenpropit (10 μM) groups. (*b*) Statistical analyses of MI of theta–high gamma coupling during the habituation trial and spatial-change trial in vehicle, triprolidine, ranitidine, and clobenpropit groups. ***$P < 0.001$.

ranitidine, $P_{\text{presentation vs. test}} < 0.05$, clobenpropit, $P_{\text{presentation vs. test}} < 0.01$; presentation trial, $P_{\text{vehicle vs. triprolidine}} < 0.001$, $P_{\text{triproline vs. ranitidine}} < 0.001$, $P_{\text{triprolidine vs. clobenpropit}} < 0.05$, test trial, $P_{\text{vehicle vs. triprolidine}} < 0.001$, $P_{\text{triproline vs. ranitidine}} < 0.001$, $P_{\text{triprolidine vs. clobenpropit}} < 0.05$, $n = 6$ rats). It is worth noting that the H3R antagonist clobenpropit (10 μM) significantly decreased the theta–high gamma coupling during habituation, but that the elevation of theta–high gamma coupling during spatial exploration was not affected. All these data show that the histamine-enhanced theta modulation of spiking and high gamma oscillations is strongly consistent with successful execution of spatial recognition, which indicates possible in vivo mechanisms for histaminergic regulation of spatial recognition.

Discussion

The entorhinal cortex is the gateway for information flow between hippocampus and other cortices, and encodes the spatial representations in the brain (Witterand Moser 2006; van Strien et al. 2009). Accurate spatial representation relies on a satisfactory arousal state. The present study, using multichannel recordings and neuropharmacological methods, reveals that histaminergic input increases the neuronal firing rate and power of local theta and high gamma oscillations in the sMEC. Although the encoding of grid cells and border cells was not shown to be regulated by histamine from our data, the theta locking strength of spiking and high gamma oscillations were enhanced. The histamine-mediated increase of theta modulation of neural activities is strongly consistent with proper spatial recognition (Fig. 9).

Role of H1Rs and H3Rs in Histamine-Mediated Neural Excitability and Local Oscillatory Activities in the sMEC In Vivo

In the central nervous system, H1Rs and H2Rs are mainly expressed in the postsynapses, while H3Rs are considered to be located presynaptically, which is important for regulating the release of other neurotransmitters or histamine itself (Panula and Nuutinen 2013). With consideration of our in vitro results, we speculate that, in vivo, the activation of postsynaptic H1Rs mainly depolarizes the membrane potential. Depolarization facilitates the excitation of principal neurons, which is reflected by the increased firing rates, and, therefore, information can be easily integrated into the sMEC. The role of H3Rs in the sMEC seems more complex. Previous studies identified diverse functions of presynaptic H3R activation in the central nervous system. In addition to the inhibition of presynaptic histamine release (Giannoni et al. 2010; Flik et al. 2011), H3Rs also mediate the decreased release of glutamate (Molina-Hernandez et al. 2001), acetylcholine (Medhurst et al. 2007), noradrenaline (Di Carlo et al. 2000), and dopamine (Fox et al. 2005). In the sMEC slice, we found that the activation of H3Rs inhibits presynaptic GABA release, which is consistent with findings in slices of substantia nigra pars reticulata (Garcia et al. 1997) and striatum (Arias-Montano et al. 2001). In vivo, the sMEC receives various types of excitatory inputs, such as the above-mentioned acetylcholinergic, noradrenalinergic, dopaminergic, and serotoninergic inputs; however, whether activation of H3Rs in the sMEC would influence the activities of other arousal-promoting systems needs to be further clarified.

Neuronal activity generates a diversity of local oscillations (Buzsaki and Wang 2012; Pignatelli et al. 2012; Xu et al. 2016). The local theta and high gamma oscillations are representations of information encoded in the sMEC. Previous studies demonstrated that theta oscillations set the temporal window for information transmission between entorhinal cortex and hippocampus (Mizuseki et al. 2009). Our results showed that histamine increased the theta and the high gamma power, indicating a role of the histaminergic system in enhancing the encoding of information in the sMEC. The local high gamma oscillations are also closely linked to information flow between entorhinal cortex and hippocampus, which is consistent with successful spatial working memory (Colgin et al. 2009; Yamamoto et al. 2014). Interestingly, the local delta power was decreased after histamine infusion in the sMEC. Delta oscillations are prominent during inactivity and slow wave sleep, while theta or gamma oscillations are dominant during active wakefulness (Chrobak and Buzsaki 1998; Hahn et al. 2012). The decreased delta power and increased theta and high gamma power indicated the transformation from slow oscillatory activities to faster oscillations in the sMEC, which is beneficial for the encoding of spatial information. This

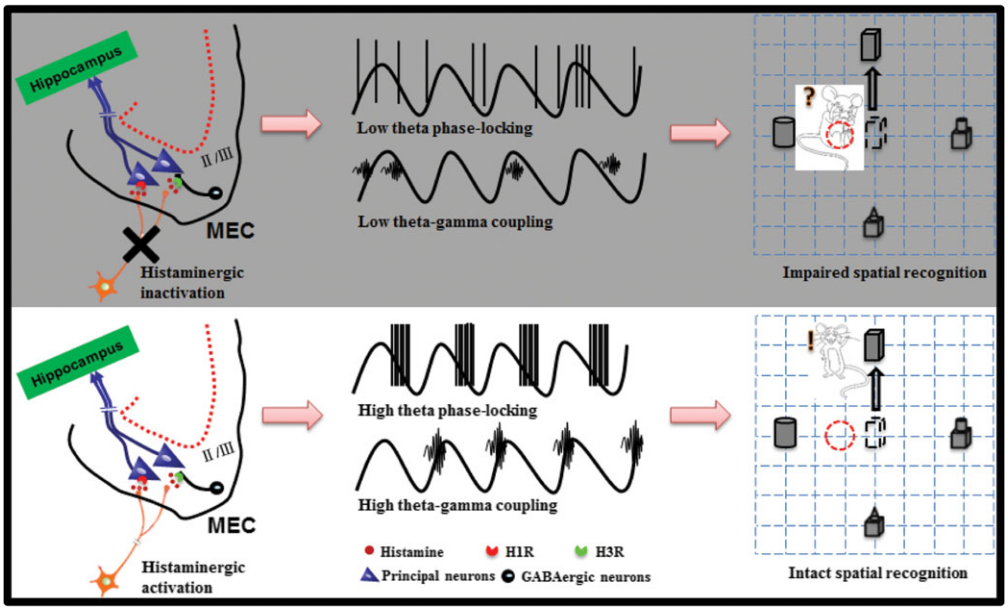

Figure 9. A schematic illustration of how the histaminergic system contributes to theta-modulated spiking and high gamma oscillations, and its correlation with spatial recognition performance. Up panel: if there is no histaminergic input, the spikes and high gamma oscillations in the sMEC are loosely locked to theta oscillations, leading to impaired spatial recognition performance. Bottom panel: by activation of H1Rs and H3Rs, histamine up-regulates neural excitability and facilitates synaptic transmission in the sMEC, the spikes and high gamma oscillations are tightly locked to theta phase, thus ensuring the intact ability of spatial recognition.

phenomenon further supports the role of histamine in up-regulating neuronal excitability and promoting entorhinal arousal. Both H1Rs and H3Rs are involved in histamine-induced elevation of theta and high gamma power. At present, the precise mechanisms underlying the H1R and H3R mediated elevation of theta and high gamma oscillations remain largely unknown, and should be clarified in the future.

Interestingly, during the freely moving test, we did not observe behavioral changes, such as the duration of grooming, number of rearing actions, movement distance, and speed of rats, or any other obvious abnormal behavior after administration of histamine or its receptor antagonists. Even so, we could not rule out the possibility that histamine regulates specific behaviors, because no standards or designs for defining specific behaviors were used in these tests. To verify the role of the histaminergic system in the sMEC, the aforementioned spatial recognition tests were applied in this study.

Histaminergic Input and Activity of Spatially Tuned Neurons in the sMEC

Since the discovery of grid cells and border cells (Fyhn et al. 2004; Hafting et al. 2005; Solstad et al. 2008), substantial effort has been made to uncover the underlying mechanisms of grid cells or border cells, and factors that regulate the activity of these neurons. Especially for grid cells, an apparent membrane potential theta oscillation was observed during spatial navigation (Schmidt-Hieber and Hausser 2013), and the firing of grid cells was tightly phase-locked to local theta oscillations (Tang et al. 2014). Thus, theta oscillations are probably a basis for grid cell activity. Inactivation of medial septum (MS) (Brandon et al. 2011; Koenig et al. 2011), blocking the cholinergic inputs (Newman et al. 2014), or hippocampal excitatory inputs (Bonnevie et al. 2013) significantly decreased the local theta power in the sMEC and disrupted the firing fields of grid cells. In our study, we found negative effect of histamine on the spatial firing of grid and border cells although an increase in the theta power. This finding reflects a distinct neuromodulatory role of histaminergic system compared with other inputs in the sMEC. The response ratio of histamine was about 76% in vitro (He et al. 2016) and 51% in vivo. It is possible that histaminergic system preferentially innervates the non-grid cells, and avoids targeting the grid cell group which occupies only about 10% of neurons in the sMEC (Tang et al. 2014). Under this condition, it is possible that histamine induces a general increase in the theta power reflecting its regulation of nongrid cells without affecting the grid properties. As for the MS-projecting system, it might target on both the grid cell and non-grid cell types. Thus, inactivation of MS altered theta power contributed by both cell types and was always accompanied by changes in functional properties of grid cells. Comparison of the differences between the cholinergic and histaminergic systems implies distinctive mechanisms of the arousal-promoting systems in the integration of the information in the sMEC. Moreover, the protocol of food deprivation was used in our experiments; this could probably enhance the arousal state and bias the results. However, if food deprivation increased arousal, the histaminergic tone would be much higher than that in non-food deprivation conditions. Under this condition, administration of histamine receptor antagonists would be much more effective. Because we found no significant effects of histamine receptor antagonists on the encoding of grid cells and border cells, it is speculated that the negative effects of the histaminergic modulation of spatial coding were unlikely to be due to the fact that the food deprivation treatment compromised the results.

Histamine-Enhanced Theta Phase-Locking of Spikes and Theta–High Gamma Coupling during Spatial Recognition

The theta phase-locking of spiking (Siapas et al. 2005; O'Neill et al. 2013; Spellman et al. 2015) and theta–gamma coupling (Sirota et al. 2008) in spatial learning and memory have been

identified in many other brain regions, especially the hippocampus and the prefrontal cortex. In the early 1990s, theta-modulated spiking and gamma oscillations were observed in the sMEC during spatial exploration (Chrobak and Buzsaki 1994, 1998). Because theta phase provides the temporal code in entorhinal–hippocampal circuits (Hafting et al. 2008; Mizuseki et al. 2009; Climer et al. 2013), it is speculated that histaminergic inputs in the sMEC may facilitate the information flow (enhanced theta power and locking strength) within these circuits, concentrating the spikes in the preferred phase, and, therefore, playing a role in elevating information processing efficiency. It is worth noting that infusion of the H1R antagonist triprolidine decreased the theta phase-locking of putative principal neurons. Because triprolidine itself reduced the local theta power, one reasonable explanation for the reduced theta phase-locking of putative principal neurons is due to the histaminergic modulation of the theta oscillation. In the present study, the oscillation signal was not preselected according to the oscillation amplitude when conducting the analysis of the spike phase-locking to theta. Thus, we cannot exclude other factors affecting neuronal firing might also affect spike phase-locking to theta, and future studies with preselecting signals would be helpful to clarify this issue. The decreased theta power could also be attributed to reduced activity. However, in our experiments, the activity of rats was not affected by triprolidine treatment. In any circumstance, the final effect of blocking H1Rs is decreased theta phase-locking of putative principal neurons, which implies lower efficiency of information encoding. Theta–nested gamma oscillations are thought to be the coding patterns of coordinated activity within the sMEC, or between the sMEC and hippocampus (Colgin et al. 2009; Buzsaki and Wang 2012). Interestingly, Hasselmo et al. recently found a role for theta–gamma coupling in high-speed encoding (Newman et al. 2013). The inhibition of cholinergic input by scopolamine decreased the coupling between the theta phase and the gamma amplitude, as well as the proportion of high speed during movement. The histaminergic system in the sMEC also enhances the strength of theta–high gamma coupling. However, we did not find a significant change in rats' speed during 2D spatial explorations.

Spatial recognition requires integration of diverse spatial information, in which the sMEC plays a major role (Van Cauter et al. 2013). Consistent with previous studies (Van Cauter et al. 2013; Morrissey and Takehara-Nishiuchi 2014), our results showed that the histaminergic system in the sMEC is involved in spatial recognition, but not novel object recognition. Interestingly, during the recognition of a changed spatial configuration, the strength of theta-modulated neuronal spiking and high gamma oscillations increased, suggesting that theta-regulated sMEC neural activities are strongly linked to spatial recognition. Blocking the histaminergic input with H1R antagonists resulted in decreased theta phase-locking of spikes among a significant proportion of neurons, and reduced theta–high gamma coupling in the sMEC, along with impaired spatial recognition. In the presence of H1R antagonists, the increased theta modulation of neural activities during spatial recognition was diminished, further supporting the assumption that histamine-mediated enhancement of theta phase-locking of spikes and theta–high gamma coupling in the sMEC are probably the in vivo mechanisms underlying histaminergic modulation of spatial recognition. Considering the role of H3Rs, it is intriguing that their inhibition decreased the theta-modulated high gamma oscillations, but failed to affect the spatial recognition performance and the corresponding elevation of theta–high gamma coupling. We speculated that in the sMEC, H1Rs, but not H3Rs, play a major role in histamine-mediated effects. They determine the final contribution of histaminergic input and its functional relevance in the sMEC. The H3Rs are possibly local regulators of the histaminergic system or other arousal-promoting systems involved in the encoding of information in the sMEC.

It is well known that animal behaviors are modulated by arousal states. Our results provide new insights into the role of arousal-promoting systems in the modulation of cognitive functions. On one hand, the activity of the histaminergic system maintains sufficient wakefulness and attention, while, on the other hand, the histaminergic neurons provide sustained excitatory inputs to the sMEC and enhance information encoding, which is strongly linked to intact behavioral functions. Impairments of the histaminergic system, which are observed in cognitive dysfunctions (Arrang 2007; Yanai and Tashiro 2007; Hu et al. 2017), probably lead to disrupted ongoing information encoding, and eventually to disturbed behavioral performance.

Supplementary Material

Supplementary material is available at *Cerebral Cortex* online.

Funding

This work was supported by grants from the National Natural Science Foundation of China (Nos. 81501146 and 31500862).

Notes

We appreciate Prof. Luis de Lecea, associate Prof. Philippe Mourrain and Dr Suszie Tyree in Department of Psychiatry and Behavioral Sciences, Stanford University, California, USA, for great help in revising the manuscript. We also thank Dr Guangyan Wu from Department of Physiology, Third Military Medical University, Chongqing, China, for providing the primary antibodies for c-fos protein. *Conflict of Interest*: None declared.

References

Airaksinen MS, Panula P. 1988. The histaminergic system in the guinea pig central nervous system: an immunocytochemical mapping study using an antiserum against histamine. J Comp Neurol. 273:163–186.

Arias-Montano JA, Floran B, Garcia M, Aceves J, Young JM. 2001. Histamine H(3) receptor-mediated inhibition of depolarization-induced, dopamine D(1) receptor-dependent release of [(3)H]-gamma-aminobutryic acid from rat striatal slices. Br J Pharmacol. 133:165–171.

Arrang JM. 2007. Histamine and schizophrenia. Int Rev Neurobiol. 78:247–287.

Ballinger EC, Ananth M, Talmage DA, Role LW. 2016. Basal forebrain cholinergic circuits and signaling in cognition and cognitive decline. Neuron. 91:1199–1218.

Bonnevie T, Dunn B, Fyhn M, Hafting T, Derdikman D, Kubie JL, Roudi Y, Moser EI, Moser MB. 2013. Grid cells require excitatory drive from the hippocampus. Nat Neurosci. 16: 309–317.

Brandon MP, Bogaard AR, Libby CP, Connerney MA, Gupta K, Hasselmo ME. 2011. Reduction of theta rhythm dissociates grid cell spatial periodicity from directional tuning. Science. 332:595–599.

Buzsaki G. 2004. Large-scale recording of neuronal ensembles. Nat Neurosci. 7:446–451.

Buzsaki G, Wang XJ. 2012. Mechanisms of gamma oscillations. Annu Rev Neurosci. 35:203–225.

Canolty RT, Edwards E, Dalal SS, Soltani M, Nagarajan SS, Kirsch HE, Berger MS, Barbaro NM, Knight RT. 2006. High gamma power is phase-locked to theta oscillations in human neocortex. Science. 313:1626–1628.

Chrobak JJ, Buzsaki G. 1994. Selective activation of deep layer (V-VI) retrohippocampal cortical neurons during hippocampal sharp waves in the behaving rat. J Neurosci. 14: 6160–6170.

Chrobak JJ, Buzsaki G. 1998. Gamma oscillations in the entorhinal cortex of the freely behaving rat. J Neurosci. 18:388–398.

Cilz NI, Kurada L, Hu B, Lei S. 2014. Dopaminergic modulation of GABAergic transmission in the entorhinal cortex: concerted roles of alpha1 adrenoreceptors, inward rectifier K^+, and T-type Ca^{2+} channels. Cereb Cortex. 24:3195–3208.

Climer JR, Newman EL, Hasselmo ME. 2013. Phase coding by grid cells in unconstrained environments: two-dimensional phase precession. Eur J Neurosci. 38:2526–2541.

Colgin LL, Denninger T, Fyhn M, Hafting T, Bonnevie T, Jensen O, Moser MB, Moser EI. 2009. Frequency of gamma oscillations routes flow of information in the hippocampus. Nature. 462:353–357.

Dejean C, Courtin J, Karalis N, Chaudun F, Wurtz H, Bienvenu TC, Herry C. 2016. Prefrontal neuronal assemblies temporally control fear behaviour. Nature. 535:420–424.

Di Carlo G, Ghi P, Orsetti M. 2000. Effect of R-(-)-alpha-methylhistamine and thioperamide on in vivo release of norepinephrine in the rat hippocampus. Prog Neuropsychopharmacol Biol Psychiatry. 24:275–284.

Flik G, Dremencov E, Cremers TI, Folgering JH, Westerink BH. 2011. The role of cortical and hypothalamic histamine-3 receptors in the modulation of central histamine neurotransmission: an in vivo electrophysiology and microdialysis study. Eur J Neurosci. 34:1747–1755.

Fox GB, Esbenshade TA, Pan JB, Radek RJ, Krueger KM, Yao BB, Browman KE, Buckley MJ, Ballard ME, Komater VA, et al. 2005. Pharmacological properties of ABT-239 [4-(2-{2-[(2R)-2-Methylpyrrolidinyl]ethyl}-benzofuran-5-yl)benzonitrile]: II. Neurophysiological characterization and broad preclinical efficacy in cognition and schizophrenia of a potent and selective histamine H3 receptor antagonist. J Pharmacol Exp Ther. 313:176–190.

Frank LM, Brown EN, Wilson MA. 2001. A comparison of the firing properties of putative excitatory and inhibitory neurons from CA1 and the entorhinal cortex. J Neurophysiol. 86: 2029–2040.

Fyhn M, Molden S, Witter MP, Moser EI, Moser MB. 2004. Spatial representation in the entorhinal cortex. Science. 305: 1258–1264.

Garcia M, Floran B, Arias-Montano JA, Young JM, Aceves J. 1997. Histamine H3 receptor activation selectively inhibits dopamine D1 receptor-dependent [3H]GABA release from depolarization-stimulated slices of rat substantia nigra pars reticulata. Neuroscience. 80:241–249.

Giannoni P, Medhurst AD, Passani MB, Giovannini MG, Ballini C, Corte LD, Blandina P. 2010. Regional differential effects of the novel histamine H3 receptor antagonist 6-[(3-cyclobutyl-2,3,4,5-tetrahydro-1H-3-benzazepin-7-yl)oxy]-N-methyl-3-pyridine carboxamide hydrochloride (GSK189254) on histamine release in the central nervous system of freely moving rats. J Pharmacol Exp Ther. 332:164–172.

Haas HL, Sergeeva OA, Selbach O. 2008. Histamine in the nervous system. Physiol Rev. 88:1183–1241.

Hafting T, Fyhn M, Bonnevie T, Moser MB, Moser EI. 2008. Hippocampus-independent phase precession in entorhinal grid cells. Nature. 453:1248–1252.

Hafting T, Fyhn M, Molden S, Moser MB, Moser EI. 2005. Microstructure of a spatial map in the entorhinal cortex. Nature. 436:801–806.

Haghparast A, Naderi N, Khani A, Lashgari R, Motamedi F. 2010. Formalin-induced differential activation of nucleus cuneiformis neurons in the rat: an electrophysiological study. J Pain. 11:32–43.

Hahn TT, McFarland JM, Berberich S, Sakmann B, Mehta MR. 2012. Spontaneous persistent activity in entorhinal cortex modulates cortico-hippocampal interaction in vivo. Nat Neurosci. 15:1531–1538.

Harris KD, Henze DA, Csicsvari J, Hirase H, Buzsaki G. 2000. Accuracy of tetrode spike separation as determined by simultaneous intracellular and extracellular measurements. J Neurophysiol. 84:401–414.

He C, Luo F, Chen X, Chen F, Li C, Ren S, Qiao Q, Zhang J, de Lecea L, Gao D, et al. 2016. Superficial layer-specific histaminergic modulation of medial entorhinal cortex required for spatial learning. Cereb Cortex. 26:1590–1608.

Hu ML, Zong XF, Mann JJ, Zheng JJ, Liao YH, Li ZC, He Y, Chen XG, Tang JS. 2017. A review of the functional and anatomical default mode network in Schizophrenia. Neurosci Bull. 33: 73–84.

Koenig J, Linder AN, Leutgeb JK, Leutgeb S. 2011. The spatial periodicity of grid cells is not sustained during reduced theta oscillations. Science. 332:592–595.

Kraus MM, Prast H, Philippu A. 2013. Influence of the hippocampus on amino acid utilizing and cholinergic neurons within the nucleus accumbens is promoted by histamine via H(1) receptors. Br J Pharmacol. 170:170–176.

Lin JS. 2000. Brain structures and mechanisms involved in the control of cortical activation and wakefulness, with emphasis on the posterior hypothalamus and histaminergic neurons. Sleep Med Rev. 4:471–503.

Lin JS, Anaclet C, Sergeeva OA, Haas HL. 2011. The waking brain: an update. Cell Mol Life Sci. 68:2499–2512.

Lu Y, Zhong C, Wang L, Wei P, He W, Huang K, Zhang Y, Zhan Y, Feng G. 2016. Optogenetic dissection of ictal propagation in the hippocampal-entorhinal cortex structures. Nat Commun. 7:10962.

McDonald JH. 2014. Handbook of biological statistics. 3rd ed. Baltimore, Maryland, USA: Sparky House Publishing. p. 59–67.

Medhurst AD, Briggs MA, Bruton G, Calver AR, Chessell I, Crook B, Davis JB, Davis RP, Foley AG, Heslop T, et al. 2007. Structurally novel histamine H3 receptor antagonists GSK207040 and GSK334429 improve scopolamine-induced memory impairment and capsaicin-induced secondary allodynia in rats. Biochem Pharmacol. 73:1182–1194.

Mizuseki K, Sirota A, Pastalkova E, Buzsaki G. 2009. Theta oscillations provide temporal windows for local circuit computation in the entorhinal-hippocampal loop. Neuron. 64:267–280.

Molina-Hernandez A, Nunez A, Sierra JJ, Arias-Montano JA. 2001. Histamine H3 receptor activation inhibits glutamate release from rat striatal synaptosomes. Neuropharmacology. 41:928–934.

Morrissey MD, Takehara-Nishiuchi K. 2014. Diversity of mnemonic function within the entorhinal cortex: a meta-analysis of rodent behavioral studies. Neurobiol Learn Mem. 115:95–107.

Newman EL, Climer JR, Hasselmo ME. 2014. Grid cell spatial tuning reduced following systemic muscarinic receptor blockade. Hippocampus. 24:643–655.

Newman EL, Gillet SN, Climer JR, Hasselmo ME. 2013. Cholinergic blockade reduces theta-gamma phase amplitude coupling and speed modulation of theta frequency consistent with behavioral effects on encoding. J Neurosci. 33:19635–19646.

Newman EL, Hasselmo ME. 2014. Grid cell firing properties vary as a function of theta phase locking preferences in the rat medial entorhinal cortex. Front Syst Neurosci. 8:193.

O'Neill PK, Gordon JA, Sigurdsson T. 2013. Theta oscillations in the medial prefrontal cortex are modulated by spatial working memory and synchronize with the hippocampus through its ventral subregion. J Neurosci. 33:14211–14224.

Otani S, Bai J, Blot K. 2015. Dopaminergic modulation of synaptic plasticity in rat prefrontal neurons. Neurosci Bull. 31: 183–190.

Ozkurt TE, Schnitzler A. 2011. A critical note on the definition of phase-amplitude cross-frequency coupling. J Neurosci Methods. 201:438–443.

Panula P, Nuutinen S. 2013. The histaminergic network in the brain: basic organization and role in disease. Nat Rev Neurosci. 14:472–487.

Panula P, Rinne J, Kuokkanen K, Eriksson KS, Sallmen T, Kalimo H, Relja M. 1998. Neuronal histamine deficit in Alzheimer's disease. Neuroscience. 82:993–997.

Pastoll H, Solanka L, van Rossum MC, Nolan MF. 2013. Feedback inhibition enables theta-nested gamma oscillations and grid firing fields. Neuron. 77:141–154.

Pignatelli M, Beyeler A, Leinekugel X. 2012. Neural circuits underlying the generation of theta oscillations. J Physiol Paris. 106:81–92.

Quilichini P, Sirota A, Buzsaki G. 2010. Intrinsic circuit organization and theta-gamma oscillation dynamics in the entorhinal cortex of the rat. J Neurosci. 30:11128–11142.

Ray S, Naumann R, Burgalossi A, Tang Q, Schmidt H, Brecht M. 2014. Grid-layout and theta-modulation of layer 2 pyramidal neurons in medial entorhinal cortex. Science. 343:891–896.

Reagh ZM, Yassa MA. 2014. Object and spatial mnemonic interference differentially engage lateral and medial entorhinal cortex in humans. Proc Natl Acad Sci USA. 111:E4264–E4273.

Sargolini F, Fyhn M, Hafting T, McNaughton BL, Witter MP, Moser MB, Moser EI. 2006. Conjunctive representation of position, direction, and velocity in entorhinal cortex. Science. 312:758–762.

Schmidt-Hieber C, Hausser M. 2013. Cellular mechanisms of spatial navigation in the medial entorhinal cortex. Nat Neurosci. 16:325–331.

Siapas AG, Lubenov EV, Wilson MA. 2005. Prefrontal phase locking to hippocampal theta oscillations. Neuron. 46:141–151.

Sirota A, Montgomery S, Fujisawa S, Isomura Y, Zugaro M, Buzsaki G. 2008. Entrainment of neocortical neurons and gamma oscillations by the hippocampal theta rhythm. Neuron. 60:683–697.

Solstad T, Boccara CN, Kropff E, Moser MB, Moser EI. 2008. Representation of geometric borders in the entorhinal cortex. Science. 322:1865–1868.

Song YN, Li HZ, Zhu JN, Guo CL, Wang JJ. 2006. Histamine improves rat rota-rod and balance beam performances through H(2) receptors in the cerebellar interpositus nucleus. Neuroscience. 140:33–43.

Spellman T, Rigotti M, Ahmari SE, Fusi S, Gogos JA, Gordon JA. 2015. Hippocampal-prefrontal input supports spatial encoding in working memory. Nature. 522:309–314.

Sun C, Kitamura T, Yamamoto J, Martin J, Pignatelli M, Kitch LJ, Schnitzer MJ, Tonegawa S. 2015. Distinct speed dependence of entorhinal island and ocean cells, including respective grid cells. Proc Natl Acad Sci USA. 112:9466–9471.

Tadel F, Baillet S, Mosher JC, Pantazis D, Leahy RM. 2011. Brainstorm: a user-friendly application for MEG/EEG analysis. Comput Intell Neurosci. 2011:879716.

Tang Q, Burgalossi A, Ebbesen CL, Ray S, Naumann R, Schmidt H, Spicher D, Brecht M. 2014. Pyramidal and stellate cell specificity of grid and border representations in layer 2 of medial entorhinal cortex. Neuron. 84:1191–1197.

Tang Q, Ebbesen CL, Sanguinetti-Scheck JI, Preston-Ferrer P, Gundlfinger A, Winterer J, Beed P, Ray S, Naumann R, Schmitz D, et al. 2015. Anatomical organization and spatiotemporal firing patterns of layer 3 neurons in the rat medial entorhinal cortex. J Neurosci. 35:12346–12354.

Thakkar MM. 2011. Histamine in the regulation of wakefulness. Sleep Med Rev. 15:65–74.

Tort AB, Komorowski RW, Manns JR, Kopell NJ, Eichenbaum H. 2009. Theta-gamma coupling increases during the learning of item-context associations. Proc Natl Acad Sci USA. 106: 20942–20947.

Tort AB, Kramer MA, Thorn C, Gibson DJ, Kubota Y, Graybiel AM, Kopell NJ. 2008. Dynamic cross-frequency couplings of local field potential oscillations in rat striatum and hippocampus during performance of a T-maze task. Proc Natl Acad Sci USA. 105:20517–20522.

Van Cauter T, Camon J, Alvernhe A, Elduayen C, Sargolini F, Save E. 2013. Distinct roles of medial and lateral entorhinal cortex in spatial cognition. Cereb Cortex. 23:451–459.

van Strien NM, Cappaert NL, Witter MP. 2009. The anatomy of memory: an interactive overview of the parahippocampal-hippocampal network. Nat Rev Neurosci. 10:272–282.

Wang DV, Yau HJ, Broker CJ, Tsou JH, Bonci A, Ikemoto S. 2015. Mesopontine median raphe regulates hippocampal ripple oscillation and memory consolidation. Nat Neurosci. 18: 728–735.

Witter MP, Moser EI. 2006. Spatial representation and the architecture of the entorhinal cortex. Trends Neurosci. 29: 671–678.

Xiao Z, Deng PY, Rojanathammanee L, Yang C, Grisanti L, Permpoonputtana K, Weinshenker D, Doze VA, Porter JE, Lei S. 2009a. Noradrenergic depression of neuronal excitability in the entorhinal cortex via activation of TREK-2 K^+ channels. J Biol Chem. 284:10980–10991.

Xiao Z, Deng PY, Yang C, Lei S. 2009b. Modulation of GABAergic transmission by muscarinic receptors in the entorhinal cortex of juvenile rats. J Neurophysiol. 102:659–669.

Xu Y, Wang L, Liu YZ, Yang Y, Xue X, Wang Z. 2016. GABAergic interneurons are required for generation of slow CA1 oscillation in rat hippocampus. Neurosci Bull. 32:363–373.

Yamamoto J, Suh J, Takeuchi D, Tonegawa S. 2014. Successful execution of working memory linked to synchronized high-frequency gamma oscillations. Cell. 157:845–857.

Yanai K, Tashiro M. 2007. The physiological and pathophysiological roles of neuronal histamine: an insight from human positron emission tomography studies. Pharmacol Ther. 113:1–15.

Yang QZ, Hatton GI. 1997. Electrophysiology of excitatory and inhibitory afferents to rat histaminergic tuberomammillary nucleus neurons from hypothalamic and forebrain sites. Brain Res. 773:162–172.

Yang Y, Wang ZH, Jin S, Gao D, Liu N, Chen SP, Zhang S, Liu Q, Liu E, Wang X, et al. 2016. Opposite monosynaptic scaling of BLP-vCA1 inputs governs hopefulness- and helplessness-modulated spatial learning and memory. Nat Commun. 7:11935.

Yu C, Shen Y, Xu L, Zhu Y, Zhuge Z, Huang Y, Henk T, Rob L, Wei E, Chen Z. 2006. Effect of endogenous histamine in the ventral hippocampus on fear memory deficits induced by scopolamine as evaluated by step-through avoidance response in rats. Physiol Behav. 87:687–693.

Zarrindast MR, Taheri S, Rezayof A. 2010. The effects of histaminergic agents in the nucleus accumbens of rats in the elevated plus-maze test of anxiety. Iran J Psychiatry. 5:11–17.

Zha X, Xu X. 2015. Dissecting the hypothalamic pathways that underlie innate behaviors. Neurosci Bull. 31:629–648.